universität wien

MASTERARBEIT / MASTER'S THESIS

Titel der Masterarbeit / Title of the Master's Thesis

„Correlated wave function methods for small molecules“

verfasst von / submitted by

Moritz Humer BSc

angestrebter akademischer Grad / in partial fulfilment of the requirements for the degree of

Master of Science (MSc)

Wien, 2021 / Vienna, 2021

Studienkennzahl lt. Studienblatt / degree programme code as it appears on the student record sheet:	A 066 876
Studienrichtung lt. Studienblatt / degree programme as it appears on the student record sheet:	Masterstudium Physik
Betreut von / Supervisor:	Univ.-Prof. Dipl.Ing. Dr. Georg Kresse
Mitbetreut von / Co-Supervisor:	

Abstract

The main topic of this thesis is the treatment of correlation energies using computational many-body methods. Because conventional methods such as Hartree-Fock or density functional theory completely neglect or only empirically approximate correlation effects, post-Kohn-Sham methods are becoming progressively more attractive. One of these is the random-phase approximation (RPA), which is discussed and derived as a natural first-order approximation in the adiabatic-connection fluctuation-dissipation theory. Since all correlated wave function methods involve virtual states, i.e. unoccupied orbitals of an underlying mean-field calculation, the most compact set of single-particle orbitals is discussed: so-called natural orbitals. These are the eigenfunctions of the density matrix and are ordered by their importance in sampling the virtual space. Since their calculation requires the knowledge of the full many-body wave function, approximate natural orbitals, obtained within the random-phase approximation (RPA-NOs), are discussed.
The second part of the thesis focuses on the calculation of atomization energies for a small set of molecules using the random-phase approximation. The calculations have been performed using the Vienna Ab initio Simulation Package (VASP). The molecules have been selected from the G2 neutral test set, which involves elements up to the third period. This set is used for bench-marking in quantum chemistry, because its molecular energies are well-established. Published results by Bates et al. [1] are used to assess the quality of the obtained RPA atomization energies. Multiple pseudo-potentials have been tested, checking for their accuracy and convergence rate with respect to both the cell size and plane-wave cutoff. Further, extrapolation methods have been evaluated to improve the RPA correlation energies. Instead of plane-waves also RPA-NOs have been used as a basis to calculate atomization energies within the RPA. Their convergence with respect to the number of used natural orbitals is evaluated. Since it is not obvious how to select the natural orbital basis sets for the atoms and the corresponding molecule, two methods to obtain truncated sets of natural orbitals are compared. Finally, the RPA has been used to calculate lattice constants of few solids using both natural orbitals and plane-waves. The results are compared to HF lattice constants and the convergence with respect to the number of orbitals is investigated.

Kurzfassung

In dieser Arbeit wird die Handhabung von Korrelationsenergien in computergestützten Viel-Teilchen Methoden besprochen. Post-Kohn-Sham Methoden werden immer attraktiver, da in konventionellen Methoden wie Hartree-Fock oder Dichtefunktionalstheorie Korrelationseffekte ignoriert oder nur empirisch angenähern werden. Eine dieser post Kohn-Sham Methoden ist die random-phase Approximation (RPA). Diese wird im Rahmen der adiabatic-connection fluctuation-dissipation Theorie hergeleitet und diskutiert. Da alle korrelierten Wellenfunktionsmethoden virtuelle Zustände beinhalten, i.e. unbesetzte Orbitale einer zugrundeliegenden mean-field Rechnung, wird das kompakteste Set von Ein-Teilchen Orbitalen diskutiert: so genannte natural orbitals. Diese sind die Eigenfunktionen der Dichtematrix und werden nach ihrer Bedeutsamkeit geordnet den unbesetzten Raum darzustellen. Da ihre Berechnung die Viel-Teilchen Wellenfunktion erfordert, werden im Rahmen der random-phase Approximation angenäherte natural orbitals (RPA-NOs) diskutiert.
Der zweite Teil der Arbeit befasst sich mit der Berechnung von Atomisierungsenergien kleiner Molekülen mit Hilfe der random-phase Approximation. Die Rechnungen wurden mit dem Vienna Ab initio Simulation Package (VASP) für Moleküle as dem G2 neutral test set durchgeführt. Dieses enthält Elemente bis zur dritten Periode und ist ein Standard Benchmark Set in der Quanten Chemie, weil die molekularen Energien gut etabliert sind. Publizierte Werte von Bates et al. [1] dienen als Referenz um die Genauigkeit der berechneten RPA Atomisierungsenergien zu bewerten. Des weiteren wurden mehrere pseudo Potentiale auf ihre Genauigkeit und ihr Konvergenzverhalten bezogen auf die Zellgröße und den Basissatz Cutoff verglichen. Um verbesserte RPA Korrelationsenergien zu erhalten wurden Zell- und Basissatz Extrapolations-Methoden geteste. Als Basis für die RPA Rechnungen wurden neben ebenen Wellen auch RPA-NOs genutzt und das Konvergenzverhalten der Atomisierungsenergien in Bezug auf die Anzahl der natural orbitals ausgewertet. Außerdem wurden zwei Methoden zur Konstruktion konsistenter natural orbital Basissätze für Atome und Moleküle verglichen. Abschließend wurden die Gitterkonstanten von einigen Festkörpern mit natural orbitals und ebenen Wellen in der RPA berechnet. Die Ergebnisse wurden mit HF Gitterkonstanten verglichen und das Konvergenzverhalten in Bezug auf die Anzahl der natural orbitals wurde untersucht.

Inhaltsverzeichnis

Chapter 1

Density functional theory

With the development of quantum mechanics in the early 1900s, physicists were eager to solve its equations to accurately describe atoms, molecules and solids. However, almost every real system consists of many interacting particles, which is the very core of the many-body problem. In quantum mechanics, a system is completely described by its wave function, which is a stunningly complicated object as it contains all the information on the many interactions between the various particles of the system. It is obtained by solving the many-body Schrödinger equation. However, this is virtually impossible as the wave function is too complex. Therefore, the major task of quantum physics and chemistry is to find approximate solutions to the electronic Schrödinger equation [2].
Wave function-based methods, like Hartree-Fock, try to find approximate solutions to the non-relativistic time-independent Schrödinger equation, which is equivalent to a wave function variational principle. By minimizing the expectation value $\langle\Psi|\hat{H}|\Psi\rangle$ of the Hamiltonian over some set of wavefunctions one finds the ground-state wave function and the corresponding ground-state energy. To solve the resulting equations, approximations are needed for the wave functions one minimizes over [3]. Often the minimization is restricted to a subspace of the space of many-body wave functions. The simplest antisymmetric many-body wave functions that can be used to describe an electronic ground-state are single Slater-determinants. Those describe independent particles but already incorporate exchange-effects, due to their requirement to be antisymmetric. This makes them a popular starting point for wave function-based methods. As the minimization is restricted only to a subspace of the space of full many-body wave functions, the minimum energy is just an upper bound to the exact ground-state energy [4]. One can also think about the Hartree-Fock method as finding an exact solution to an approximate one-body Hamiltonian. The approximate solution to the real many-body Hamiltonian solves the eigenvalue equation

of the one-body Hamiltonian exactly. This approximate Hamiltonian is of mean-field type, including the electrostatic Hartree interaction and a non-local one-body mean-field potential, describing exchange effects. The latter originates from the anti-symmetry of the Slater-determinants. This Hartree-Fock Hamiltonian is an approximation to the full many-body Hamiltonian, including electrostatic and exchange interaction, both modeled by a mean-field potential. In this picture, one solves the equations of an auxiliary independent particle system exactly. The solution is the HF wave function, i.e. a single Slater-determinant.

It turns out that solving the Schrödinger equation for the wave function, even if it is only an approximated one, is not the most practical approach. An N-electron wave function has in general 3 spatial and 1 spin coordinate for each electron and hence depends in total on $4N$ variables. Thus it is of great interest that the energy of an electronic system can also be written in terms of the electronic density [2]. Hohenberg and Kohn showed in their famous 1964 paper [5] that the knowledge of the one-particle electron density is sufficient to determine all properties of an electronic system. This theorem implies the existence of an energy functional solely depending on the electronic density. With a variational principle, the minimizing ground-state density and therefore all ground-state properties can be obtained. Although this formalism is in principle exact, the functional dependence of the energy on the density is unknown and therefore approximations are needed. A year later in 1965 Kohn and Sham [6] came up with a clever way to split the energy-functional. This allowed an explicit treatment of the major contributions to the energy and approximations could be applied for the remainder. This laid the foundation for the success of modern density-functional theory (DFT). It is so popular because of its computational simplicity and because the 3-dimensional density is easier to deal with than the $3N$-dimensional wave function (suppressing the spin variables) [7]. In the following section, I will discuss the foundations of density functional theory and the Kohn-Sham method.

One final note on the units used throughout this thesis: the equations are written down using Hartree atomic units [3]. They are motivated by the desire to obtain a dimensionless Schrödinger equation. This is achieved by setting

$$\frac{1}{4\pi\epsilon_0} = \hbar = e = m_e = 1, \tag{1.0.1}$$

where ϵ_0 is the vacuum permittivity, $\hbar$ is the reduced Planck's constant, e is the electric charge of an electron and m_e is its mass. The resulting length and energy units in atomic units are the Bohr radius a_0 ($5.2918 \times 10^{-11}\,\mathrm{m}$) and Hartree ($4.3598 \times 10^{-18}\,\mathrm{J}$)

respectively.

1.1 The Kohn-Sham method

All properties of an electronic system in a general external potential $v_{ext}(\mathbf{r})$ can be determined once the Hamiltonian is known. In order to write down the Hamiltonian the knowledge of the electron number N and the external potential $v_{ext}(\mathbf{r})$ is required. In their 1965 paper, Hohenberg and Kohn showed that for a given ground-state density $n_0(\mathbf{r})$ the external potential is uniquely determined up to a constant [5, 7]. Further, the ground-state density integrates to the electron number N. Therefore the full Hamiltonian is determined only by the ground-state density. This implies that e.g. the ground-state wave function and energy, the electrical polarizability and energies are all functionals of the ground-state density. Although this theorem has powerful implications, it does not provide a recipe for how to construct the energy functional. The total ground-state energy of a system can be written as

$$\begin{aligned} E_0 &= \left\langle \Psi_0 \middle| \hat{T} + \hat{V}_{ee} \middle| \Psi_0 \right\rangle + \left\langle \Psi_0 \middle| \hat{V}_{ext} \middle| \Psi_0 \right\rangle \\ &= F[n_0] + \int d\mathbf{r} v_{ext}(\mathbf{r}) n_0(\mathbf{r}), \end{aligned} \tag{1.1.1}$$

where Ψ_0 denotes the ground-state wave function and $n_0(\mathbf{r})$ the corresponding ground-state density. Further $\hat{T}$, $\hat{V}_{ee}$ and $\hat{V}_{ext}$ are the kinetic energy-, electron-electron interaction energy- and external potential operator respectively. The potential energy is then written in terms of the ground-state density of the system and a universal functional $F[n]$ is introduced

$$F[n] = \left\langle \Psi \middle| \hat{T} + \hat{V}_{ee} \middle| \Psi \right\rangle. \tag{1.1.2}$$

From the definition above it is obvious that it is a functional of the density because $\Psi[n]$ is. It is the sum of the kinetic energy functional $T[n]$ and electron-electron interaction functional $V_{ee}[n]$. Using the Rayleigh-Ritz principle for the ground-state energy, one finds that the functional (1.1.1) has a minimum, for the correct ground-state density $n_0(\mathbf{r})$ [7, 8]. The universal functional is defined for any electronic density that corresponds to some antisymmetric ground-state wave function Ψ of some Hamiltonian with local external potential. The possible densities are referred to as v-representable. This is a serious limitation, as one might go outside of definition range when applying the variational

principle [9].
Levy and Lieb derived a universal functional that is defined for a broader class of densities. Starting with the conventional Rayleigh-Ritz principle, the ground-state energy is obtained by minimizing

$$E_0 = \min_{\Psi} \left\langle \Psi \middle| \hat{H} \middle| \Psi \right\rangle . \tag{1.1.3}$$

In the constrained search approach [4, 7], the minimization over all possible N-particle wave functions Ψ is split into two separate minimizations. The outer one is performed over all trial densities, while the inner one minimizes all wave functions yielding that trial density

$$E_0 = \min_{n} \left(F[n] + \int d\mathbf{r} v_{ext}(\mathbf{r}) n(\mathbf{r}) \right) . \tag{1.1.4}$$

Note that the potential energy associated with the external potential $v(\mathbf{r})$ is excluded from the minimization over the many-body wave function because they are constraint to yield the same density and thus the same $\langle \Psi | \hat{V}_{ext} | \Psi \rangle$. Therefore the functional $F[n]$ is universal in the sense that it is the same for any N-particle systems regardless of the external potential $v_{ext}(\mathbf{r})$. The universal functional of Levy and Lieb is defined as

$$\begin{aligned} F[n] &= \min_{\Psi \to n} \left\langle \Psi \left| \hat{T} + \hat{V}_{ee} \right| \Psi \right\rangle \\ &= \left\langle \Psi^n_{min} \left| \hat{T} + \hat{V}_{ee} \right| \Psi^n_{min} \right\rangle , \end{aligned} \tag{1.1.5}$$

where Ψ^n_{min} denotes the minimizing wave function yielding a fixed trial density n. While the previous definition by Hohenberg and Kohn (1.1.2) applies only to ground-state densities, this universal functional is defined for any density that may be obtained from some antisymmetric wave function. This condition is called N-representable. Since this is a weaker condition than v-representability, this newly defined universal functional paves the way to a broader class of trial densities.
Although instructive, this approach is formal and does not yield further instructions on how to construct the universal functional. Especially the kinetic energy functional is unknown and poses a challenge to find good approximations for. Kohn and Sham came up with a clever way to split the universal functional into three major contributions. In doing so they could treat the non-interacting kinetic energy and the classical electrostatic interaction exactly, leaving only the exchange and correlation energy to be approximated [4]. Within the Kohn-Sham method, the universal energy functional $F[n]$ is written as

$$F[n] = T_s[n] + E_H[n] + E_{xc}[n]. \tag{1.1.6}$$

Here $T_s[n]$ is the non-interacting kinetic energy functional defined as the minimization over single Slater-determinants Φ yielding a fixed electronic density n

$$\begin{aligned} T_s[n] &= \min_{\Phi \to n} \left\langle \Phi \left| \hat{T} \right| \Phi \right\rangle \\ &= \left\langle \Phi^n_{min} \left| \hat{T} \right| \Phi^n_{min} \right\rangle \end{aligned} \tag{1.1.7}$$

and $E_H[n]$ is the classical electrostatic interaction energy

$$E_H[n] = \frac{1}{2} \int \int d\mathbf{r} d\mathbf{r}' \frac{n(\mathbf{r}) n(\mathbf{r}')}{|\mathbf{r} - \mathbf{r}'|}. \tag{1.1.8}$$

The benefit of this approach is that the typically large contributions to the total energy – the non-interaction kinetic energy and the Hartree energy – are treated exactly [10]. Although a wave function has been reintroduced it is a tremendous simplification since it is not the full many-body wave function Ψ but a single-determinant Φ – the Kohn-Sham wave function. The remaining non-classical interaction contributions and the difference to the true interacting kinetic energy are included in the exchange-correlation energy functional E_{xc} for which approximations are needed.

In order to deal with spin-dependent external potentials or strong spin-orbit coupling atoms, the DFT formalism can be extended from the total density to spin-densities $n_\uparrow$ and $n_\downarrow$ [4, 9]. Using the (generalized) Kohn-Sham universal functional (1.1.6) together with the energy functional (1.1.4) and minimizing with respect to single-particle orbitals $\phi_{i,\sigma}(\mathbf{r})$ (building the Kohn-Sham wave function Φ) under the constraint that they are orthonormal, one finds the spin-dependent Kohn-Sham equations

$$\left(-\frac{1}{2}\nabla^2 + v(\mathbf{r}) + \int d^3r \frac{n(\mathbf{r}')}{|\mathbf{r} - \mathbf{r}'|} + v_{xc,\sigma}([n_\uparrow, n_\downarrow], \mathbf{r}) \right) \phi_{i,\sigma}(\mathbf{r}) = \epsilon_{i,\sigma} \phi_{i,\sigma}(\mathbf{r}), \tag{1.1.9}$$

where the density $n(\mathbf{r})$ is calculated by the N occupied single-particle spin-orbitals $\{\phi_{j,\sigma}(\mathbf{r})\}_{j=1,\ldots,N}$, where σ is the spin index

$$n(\mathbf{r}) = n_\uparrow(\mathbf{r}) + n_\downarrow(\mathbf{r}) = \sum_\sigma \sum_{j=1}^{N} |\phi_{j,\sigma}(\mathbf{r})|^2. \tag{1.1.10}$$

Those are independent particle equations - similar to the Hartree equations - in an effective

potential. Thus the Kohn-Sham approach to density-functional theory is interpreted as replacing the real physical interacting system by an auxiliary system of non-interacting particles in an effective potential $v_s(\mathbf{r})$. This Kohn-Sham effective potential ensures that the ground-state density of the auxiliary system is identical to the one of the physical system. It accounts for the interaction with the external potential, a classical Hartree contribution but also depends on exchange-correlation energy functional. For more information on the Kohn-Sham equations consider reading [6, 11, 12].

In principle, if the exact exchange-correlation functional would be known, the Eqs. (1.1.9) are exact. However in practice, we need good approximations for $E_{ex}[n_\uparrow, n_\downarrow]$. The first approximation already proposed by Kohn and Sham is the local-density approximation (LDA) [6,12] or more general the local spin-density approximation (LSDA). The foundation is the observation that solids can often be considered close to the limit of the homogeneous electron gas. They proposed to approximate the local exchange-correlation energy density with that of the homogeneous electron gas of the same density. Since exchange and correlation effects are rather short ranged for densities typical for solids, the LDA is somewhat justified. Therefore one would expect the LDA to work better for solids with slow and weak density variations, for instance alkali metals. Nevertheless, the LDA works remarkably well even for very inhomogeneous systems. Note that the LDA is not self-interaction-free, as the local approximation to exchange only partially cancels the Hartree self-interaction. Since the exchange-correlation energy will in general be non-local, the LDA leaves room for improvements. LDA thus serves as a starting point and gradient corrections, taking the inhomogeneity into account, in the form of the local density gradients are added [12, 13]. Note that the generalized-gradient approximation functionals (GGA) are perfectly local. They can be visualized as a kind of Taylor expansions incorporating not only the information of the density at the given point but also its derivatives. But naively adding gradient corrections to the LDA functional leads to only modest improvements. Therefore some GGA functionals are parametrized by fitting experimental data, while others achieve the inclusion of gradient corrections without introducing experimentally fitted parameters. The latter may be applied to a wider class of systems. The most famous parameter-free GGA functional was developed by Perdew, Burke, and Ernzerhof (PBE) [14]. The last discussed class of functionals are hybrid-functionals. They are motivated by the fact that further improvements are unlikely unless a portion of exact-exchange is mixed with GGA exchange-correlation functionals [15, 16]. By mixing the non-local exact-exchange one truly incorporates non-locality into the exchange-correlation functional. Without going into too much detail on the derivation of hybrid-functionals, take for example the famous B3LYP-functional

$$E_{xc}^{B3LYP} = E_{xc}^{LSDA} + 0.2(E_x^{KS} - E_x^{LDSA}) + 0.72E_x^{B88} + 0.81E_c^{LYP} + 0.19E^{VWN}. \quad (1.1.11)$$

This mixes the exchange-correlation energy of the LSDA method with 20% of the difference between Kohn-Sham exact-exchange and the LSDA exchange energy. Then 72% of Beckes exchange potential E^{B88} [17], 81% of the Lee–Yang–Parr correlation potential E_c^{LYP} [18] and finally 19% of the Vosko–Wilk–Nusair potential E^{VWN} [19] are added. This functional yields great results and as long as one is not interested in why it is working. Nevertheless, it is desirable to find a more systematic method to calculate the exchange and correlation energies. Therefore we will have a closer look at the exchange and correlation functionals defined by Eq. (1.1.6).

1.1.1 Exchange and correlation energy functional

The exchange and correlation energy describes all the interaction effects which can not be treated exactly in density functional theory. It arises from three effects: a correction for the self-interaction appearing in the classical Hartree term, the Pauli exclusion principle, which keeps electrons with parallel spin apart, and the Coulomb correlation upon the many-body wave function. The first two effects give rise to the exchange energy while the last is responsible for the correlation energy [4]. A world without the exchange and correlation energy would drastically differ from the one we know. Therefore Kurth and Perdew referred to the exchange-correlation as nature's glue in their paper [20]. In the previous section, we have introduced the exchange-correlation functional in Eq. (1.1.6) but did not further specify what it looks like. In general, it is written as the sum of two contributions

$$\begin{aligned} E_{xc}[n] =& E_x[n] + E_c[n], \\ =& \left\langle \Psi_{min}^n \left| \hat{T} + \hat{V}_{ee} \right| \Psi_{min}^n \right\rangle - \left\langle \Phi_{min}^n \left| \hat{T} \right| \Phi_{min}^n \right\rangle - E_H[n]. \end{aligned} \quad (1.1.12)$$

Here Ψ_{min}^n denotes the minimizing many-body wave function, while Φ_{min}^n is the Kohn-Sham wave function. The exchange energy is defined as the difference between the electron-electron interaction energy evaluated with Slater-determinants and the classical Hartree energy. The exchange functional is written as

$$E_x[n] = \left\langle \Phi_{min}^n \left| \hat{V}_{ee} \right| \Phi_{min}^n \right\rangle - E_H[n]. \quad (1.1.13)$$

The definition above is general but one has to be careful which determinant is used. Since we defined the exchange energy functional within the DFT context, the obvious choice is the Kohn-Sham wave function. If the Hartree-Fock wave function is used, the Eq. (1.1.13) defines the Hartree-Fock exchange energy. In quantum chemistry, the latter is referred to as "exact exchange". The correlation functional is defined as the difference between the correct kinetic and interaction energy and the Hartree, exchange and non-interacting kinetic energy

$$E_c[n] = \left\langle \Psi^n_{min} \middle| \hat{T} + \hat{V}_{ee} \middle| \Psi^n_{min} \right\rangle - \left\langle \Phi^n_{min} \middle| \hat{T} + \hat{V}_{ee} \middle| \Phi^n_{min} \right\rangle . \tag{1.1.14}$$

Those definitions of the exchange and correlation energies are formal ones and do not yield much insight or clues, on how to construct the corresponding density functionals. For now, we cannot further simplify those expressions. First, we need to introduce the adiabatic connection formalism, which is discussed in the upcoming chapter.

1.2 Adiabatic connection formalism

The adiabatic connection was first used by Harris and Jones [21] in 1974 to derive an exact expression for the exchange and correlation energy of an inhomogeneous electron gas within the Kohn-Sham picture. This method provides a direct link between the Kohn-Sham non-interacting system and the physical system [22]. Within this formalism, the exchange-correlation energy is expressed as a coupling-strength integration and the exchange-correlation hole. The starting point is a modified electron-electron interaction. A common choice is the replacement $\frac{1}{\mathbf{r}_{12}} \to \frac{\lambda}{\mathbf{r}_{12}}$, where $\lambda \in [0, 1]$ is a coupling-strength parameter. This leads to the following interaction operator

$$\hat{V}^{\lambda}_{ee} = \sum_{i \neq j} \frac{\lambda}{\mathbf{r}_{ij}} = \lambda \hat{V}_{ee}, \tag{1.2.1}$$

where we exploited the linearity to write the parameter in front. Then the full Hamiltonian reads

$$\hat{H}^{\lambda} = \hat{T} + \lambda \hat{V}_{ee} + \hat{V}^{\lambda}_{ext}, \tag{1.2.2}$$

where $\hat{V}^{\lambda}_{ext}$ is the external potential operator imposing that the ground-state density is the physical one for all λ

$$n^{\lambda}(\mathbf{r}) = n^{\lambda}(\mathbf{r}) \,|_{\lambda=1} = n(\mathbf{r}). \tag{1.2.3}$$

It is obvious that for $\lambda = 1$ the electron-electron interaction is not scaled and therefore the physical system is recovered. Thus $\hat{V}_{ext}^{\lambda=1} = \hat{V}_{ext}$ is the real external potential. On the other end of the connection is the auxiliary Kohn-Sham system, with the effective Kohn-Sham potential constraining the electronic density to the physical one. We may also define the λ-dependent universal functional analogous to Eq. (1.1.5)

$$\begin{aligned} F^{\lambda}[n] &= \min_{\Psi \to n} \left\langle \Psi \middle| \hat{T} + \lambda \hat{V}_{ee} \middle| \Psi \right\rangle \\ &= \left\langle \Psi_{min}^{\lambda,n} \middle| \hat{T} + \lambda \hat{V}_{ee} \middle| \Psi_{min}^{\lambda,n} \right\rangle . \end{aligned} \tag{1.2.4}$$

For convenience, we will drop the indices n and min, indicating that Ψ is the minimizing wave function yielding the density n. The wave function now also depends on the coupling-strength parameter. Note that the Kohn-Sham wave is fixed via the density and thus is independent of λ. This becomes obvious by considering $F^{\lambda=0}[n]$, which is independent of λ. Following the definition of the exchange-correlation (1.1.12) from the previous chapter we write

$$\begin{aligned} E_{xc}[n] =& \left\langle \Psi^{\lambda} \middle| \hat{T} + \hat{V}_{ee} \middle| \Psi^{\lambda} \right\rangle - \left\langle \Phi \middle| \hat{T} \middle| \Phi \right\rangle - E_H[n] \\ =& F^{\lambda=1}[n] - F^{\lambda=0}[n] - E_H[n] \\ =& \int_0^1 d\lambda \frac{dF^{\lambda}[n]}{d\lambda} - E_H[n]. \end{aligned} \tag{1.2.5}$$

Here $\langle \Phi | \hat{T} | \Phi \rangle$ is just the non-interacting kinetic energy $T_s[n]$ and therefore corresponds to the universal functional without any interactions. Note that in $F^{\lambda}[n]$ both the electron-electron interaction operator and the wave function depend on the coupling-strength parameter. To evaluate the derivative on the right-hand side, we need to briefly discuss the Hellmann-Feynman theorem.

1.2.1 The Hellmann-Feynman theorem

In this section, I want to briefly discuss the derivation of the Hellmann-Feynman theorem [23] and one of its important implications. Consider a Hamiltonian $\hat{H}^{\lambda}$, which depends explicitly upon a parameter λ. We denote any of its normalized eigenfunction with Ψ^{λ} and the corresponding eigenenergy by E^{λ}. Note that, since $\hat{H}^{\lambda}$ depends explicitly on λ also any eigenfunction and eigenvalue will be a function of the parameter. Often we are interested how the energy $E^{\lambda} = \left\langle \Psi^{\lambda} \middle| \hat{H}^{\lambda} \middle| \Psi^{\lambda} \right\rangle$ depends upon the parameter λ, thus we

want to evaluate its derivative with respect to λ

$$\begin{aligned}\frac{\partial E^\lambda}{\partial \lambda} =& \frac{\partial}{\partial \lambda}\left\langle \Psi^\lambda \left| \hat{H}^\lambda \right| \Psi^\lambda \right\rangle \\ =& \left\langle \frac{\partial \Psi^\lambda}{\partial \lambda} \left| \hat{H}^\lambda \right| \Psi^\lambda \right\rangle + \left\langle \Psi^\lambda \left| \frac{\partial \hat{H}^\lambda}{\partial \lambda} \right| \Psi^\lambda \right\rangle + \left\langle \Psi^\lambda \left| \hat{H}^\lambda \right| \frac{\partial \Psi^\lambda}{\partial \lambda} \right\rangle .\end{aligned} \tag{1.2.6}$$

Since the Hamiltonian is a hermitian operator, the third term on the right hand side can be rewritten using the relation

$$\left\langle \Psi^\lambda \left| \hat{H}^\lambda \right| \frac{\partial \Psi^\lambda}{\partial \lambda} \right\rangle = \left\langle \frac{\partial \Psi^\lambda}{\partial \lambda} \left| \hat{H}^\lambda \right| \Psi^\lambda \right\rangle^* , \tag{1.2.7}$$

and thus we can use $\hat{H}^\lambda \Psi^\lambda = E^\lambda \Psi^\lambda$ to simplify both the first and the third term in Eq. (1.2.6). Since the eigenvalues of a hermitian operator are real, the equation becomes

$$\begin{aligned}\frac{\partial E^\lambda}{\partial \lambda} =& E^\lambda \left\langle \frac{\partial \Psi^\lambda}{\partial \lambda} \middle| \Psi^\lambda \right\rangle + \left\langle \Psi^\lambda \left| \frac{\partial \hat{H}^\lambda}{\partial \lambda} \right| \Psi^\lambda \right\rangle + E^\lambda \left\langle \Psi_\lambda \middle| \frac{\partial \Psi^\lambda}{\partial \lambda} \right\rangle \\ =& E^\lambda \frac{\partial}{\partial \lambda}\left\langle \Psi^\lambda \middle| \Psi^\lambda \right\rangle + \left\langle \Psi^\lambda \left| \frac{\partial \hat{H}^\lambda}{\partial \lambda} \right| \Psi^\lambda \right\rangle .\end{aligned} \tag{1.2.8}$$

Finally, due to the normalization of the eigenfunction of the Hamiltionian $\left\langle \Psi^\lambda \mid \Psi^\lambda \right\rangle = 1$ the first term in Eq. (1.2.8) drops out. This leaves us with the simple relation

$$\frac{\partial E^\lambda}{\partial \lambda} = \frac{\partial}{\partial \lambda}\left\langle \Psi^\lambda \left| \hat{H}^\lambda \right| \Psi^\lambda \right\rangle = \left\langle \Psi^\lambda \left| \frac{\partial \hat{H}^\lambda}{\partial \lambda} \right| \Psi^\lambda \right\rangle , \tag{1.2.9}$$

which is known as the Hellmann-Feynman theorem. It states that the partial derivative of the energy with respect to a parameter λ depends only on the derivative of the Hamiltonian and not on the derivative of the wave functions. Since $\hat{H}^\lambda$ consists of a kinetic- and potential energy operator, one might be led to the conclusion that an analogous equation like Eq. (1.2.9) holds for both $\hat{T}$ and $\hat{V}$ separately [23]. This is not valid as the derivation of the relation (1.2.9) relies on the fact that Ψ^λ is an eigenfunction of the Hamiltonian. Since it is neither an eigenfunction of $\hat{T}$ nor $\hat{V}$, the derivation does not work for these operators. The theorem was first proven by Schrödinger [24] in 1926 and later mentioned by many others. Hellmann [25, 26] in 1937 and Feynman [27] in 1939 separately recognized one of its best-known consequences - the so-called electrostatic theorem. Within the Born-Oppenheimer approximation, the nuclei are frozen and thus their positions $\{\mathbf{R}_I\}_{I=1,\ldots,M}$ enter the full many-body Hamiltonian just as parameters

$$\hat{H} = \sum_{i=1}^{N} -\frac{1}{2}\nabla_i^2 - \sum_{i=1}^{N}\sum_{I=1}^{M} \frac{Z_I}{|\mathbf{r}_i - \mathbf{R}_I|} + \frac{1}{2}\sum_{i\neq j=1}^{N} \frac{1}{|\mathbf{r}_i - \mathbf{r}_j|} + \frac{1}{2}\sum_{I\neq J=1}^{M} \frac{Z_I Z_J}{|\mathbf{R}_I - \mathbf{R}_J|}. \tag{1.2.10}$$

The force acting on nucleus I is given by $\mathbf{F}_I = -\partial E/\partial \mathbf{R}_I$. Since the nuclear positions are parameters in the Hamiltonian, the Hellman-Feynman theorem applies to the right-hand side. Doing the calculations yields the electrostatic theorem.

$$-\frac{\partial E}{\partial \mathbf{R}_I} = \sum_{I\neq J} \frac{Z_I Z_J (\mathbf{R}_I - \mathbf{R}_J)}{|\mathbf{R}_I - \mathbf{R}_J|^3} + \int \frac{Z_I(\mathbf{r} - \mathbf{R}_I)\rho(\mathbf{r})}{|\mathbf{r} - \mathbf{R}_I|^3} d^3r \tag{1.2.11}$$

It states that the force on nucleus I due to the other nuclei and the electrons is exactly what could be computed in classical electrostatics from the location of the other nuclei and the electronic charge density $\rho(\mathbf{r})$ [28]. By varying the nuclear positions $\{\mathbf{R}_I\}$ until the energy is a minimum and $\partial E/\partial \mathbf{R}_I = 0$ for all nuclear positions, the equilibrium geometry of a molecule or solid can be found. The Hellmann-Feynman theorem will be applied in the next section to derive the total ground-state energy in the adiabatic-connection formalism.

1.2.2 Adiabatic connection formula

Now that we had a look at the Hellmann-Feynman theorem we can finally evaluate the integrand in Eq. (1.2.5) and express the exchange-correlation energy of the physical system as

$$\begin{aligned} E_{xc}[n] &= \int_0^1 d\lambda \frac{d}{d\lambda} \left\langle \psi^\lambda \middle| \hat{T} + \lambda \hat{V}_{ee} \middle| \Psi^\lambda \right\rangle - E_H[n] \\ &= \int_0^1 d\lambda \left\langle \Psi^\lambda \middle| \hat{V}_{ee} \middle| \Psi^\lambda \right\rangle - E_H[n]. \end{aligned} \tag{1.2.12}$$

Recall that Ψ^λ is the minimizing wave function that yields the density $n(\mathbf{r})$. Further the superscript $\lambda = 1$, indicating the exchange and correlation energy of the physical system, is suppressed. Note that usually the interacting part of the kinetic energy contributes to the correlation energy (see Eq. 1.1.14) but the equation is independent of the kinetic energy. The exchange-correlation energy is expressed just as a coupling strength integral over the electron-electron interaction energy minus the classical Hartree energy. We know that the latter is given in terms of one-electron densities. Since the electron-electron interaction is

a two-body quantity, it may be expressed in terms of the pair-density $n^\lambda(\mathbf{r}, \mathbf{r}')$

$$\left\langle \Psi^\lambda \middle| \hat{V}_{ee} \middle| \Psi^\lambda \right\rangle = \int\int d\mathbf{r} d\mathbf{r}' \frac{n^\lambda(\mathbf{r}, \mathbf{r}')}{|\mathbf{r} - \mathbf{r}'|}. \tag{1.2.13}$$

Note that only the one-electron density is constant along the connection path but not necessarily the pair-density and thus depends on the coupling parameter. Further, it fulfills the following normalization condition

$$\int\int d\mathbf{r} d\mathbf{r}' n^\lambda(\mathbf{r}, \mathbf{r}') = N(N-1), \tag{1.2.14}$$

where N is the number of electrons in the system. If the electrons would be uncorrelated, i.e treated classically, the pair-density also becomes uncorrelated and is just the product of one-electron densities $n^\lambda(\mathbf{r}, \mathbf{r}') = n(\mathbf{r})n(\mathbf{r}')$. In this case, the electron-electron interaction energy (1.2.13) reduces to the classical Hartree energy. Since the one-particle densities are normalized to the number of electrons, this violates the normalization condition (1.2.14). Therefore the probability distribution of the second electron must be correlated with the position of the first one [29]. We take care of this by writing the pair-density as the classical uncorrelated contribution plus a term taking care of the electron correlations

$$n^\lambda(\mathbf{r}, \mathbf{r}') = n(\mathbf{r}) \left[n(\mathbf{r}') + n^\lambda_{xc}(\mathbf{r}', \mathbf{r}) \right]. \tag{1.2.15}$$

Here $n^\lambda_{xc}(\mathbf{r}', \mathbf{r})$ denotes the exchange-correlation hole associated with the minimizing wave function in Eq. (1.2.13). Since electrons obey Fermi statistics they are also kept apart quantum mechanically by the Pauli exclusion principle and the Coulomb correlation. These effects are accounted for by the exchange-correlation hole. From the normalization condition of the pair-density (1.2.14) one finds

$$\int d\mathbf{r}' n^\lambda_{xc}(\mathbf{r}', \mathbf{r}) = -1. \tag{1.2.16}$$

This implies that surrounding every electron location there is a depletion in the density integrating up to exactly one electron. Combining the expression for the pair-density (1.2.15) and the Hartree term, we can rewrite Eq. (1.2.12) as

$$E_{xc} = \frac{1}{2} \int_0^1 d\lambda \int\int d\mathbf{r} d\mathbf{r}' \frac{n(\mathbf{r}) n^\lambda_{xc}(\mathbf{r}', \mathbf{r})}{|\mathbf{r} - \mathbf{r}'|}. \tag{1.2.17}$$

This is the so-called adiabatic connection formula. Defining the coupling-constant averaged hole

$$\bar{n}_{xc}(\mathbf{r},\mathbf{r}') = \int_0^1 d\lambda, n_{xc}^{\lambda}(\mathbf{r},\mathbf{r}') \tag{1.2.18}$$

we can interpret the exchange-correlation energy as the one-electron density interacting with the potential energy due to the coupling constant averaged hole

$$\begin{aligned} \epsilon_{xc}(\mathbf{r}) &= \frac{1}{2}\int d\mathbf{r}' \frac{\bar{n}_{xc}(\mathbf{r},\mathbf{r}')}{|\mathbf{r}-\mathbf{r}'|} \\ E_{xc}[n] &= \int d\mathbf{r} n(\mathbf{r})\epsilon_{xc}(\mathbf{r}) \end{aligned} \tag{1.2.19}$$

The potential exchange-correlation energy ϵ_{ex} is an implicit functional of the density, as the density is required to be constant along the connection path. Therefore we can interpret $E_{ex}[n]$ as an interpolation between the exchange-correlation energy of the auxiliary and the physical system at a given density [12]. The former include exchange-only, as it is a system of independent particles described by single Slater-determinants. The latter is the fully correlated energy.

The adiabatic connection formula is an important starting point for post-Kohn-Sham methods. One of them, the random phase approximation is discussed in the next chapter.

Chapter 2

Adiabatic-connection fluctuation-dissipation theory

It is of great interest to improve on Kohn-Sham DFT and Hartree-Fock in order to include correlation effects in these methods. While in HF the exchange energy is treated exactly but no correlation effects are included, in DFT the exchange-correlation functional is approximated with variously sophisticated functionals. Examples of such approximations are the local-density approximation (LDA) or the generalized gradient approximation (GGA). Within those approximations, the exchange-correlation energy is treated as explicit functional of the density and its local gradients.

A well-established route to improve on density functionals is to identify parts of the total ground-state energy functional suitable for approximation and treat the remainder exactly [30]. Similar to the Kohn-Sham method, which treats the non-interacting energy exactly and applies approximations for the exchange-correlation energy functional, one wants to identify a zeroth-order treatment of the correlation energy. This should include the most important correlation effects and can be computed exactly. The adiabatic connection underlies most post-Kohn-Sham correlation treatments. Such a systematic approach to approximate the correlation energy of a many-body system is the random-phase approximation (RPA).

The RPA may be derived from different theoretical frameworks. A convenient starting point is the adiabatic connection formalism discussed in the previous chapter. We will use it to formally evaluate the ground-state total energy of an interacting system of particles. With the decomposition of the Kohn-Sham universal functional, we can then identify the parts already treated explicitly in DFT and are left with an expression for the exchange-correlation energy. Comparing this expression with the adiabatic connection formula we

may identify the expression for the exchange-correlation hole. The fluctuation-dissipation theorem links the exchange-correlation energy to the response properties of the system [31]. The random-phase approximation will then arise as a natural zero-order approximation of the correlation energy. Within the RPA the exchange-correlation energy is split into the exact exchange and the RPA approximation to the correlation energy. It will be discussed in the next chapter.

2.1 Interacting ground-state energy

To derive the random phase approximation, it is sufficient to start with the adiabatic connection formula (1.2.12). Nevertheless, I think it is instructive to start with a formally exact expression of the ground-state energy within the adiabatic connection framework. From there we will restrict the ground-state density along the connection to be the physical one - i.e. we will derive the random phase approximation in terms of DFT. At the end of this section, we will again find the adiabatic connection formula for the exchange-correlation energy together with a formally exact expression for the exchange-correlation hole.
The starting point is a set of coupling-strength dependent Hamiltonians

$$\hat{H}(\lambda) = \hat{H}_0 + \lambda \hat{H}_1(\lambda). \tag{2.1.1}$$

These connect a reference Hamiltonian $\hat{H}_0$ with the full many-body Hamiltonian $\hat{H}$ [31]. The perturbative two-body Hamiltonian $\hat{H}_1(\lambda)$ includes the electron-electron interaction. The parameter of the adiabatic coupling is chosen such that $\lambda \in [0, 1]$, where $\lambda = 1$ defines the physical system and $\lambda = 0$ corresponds to the non-interacting reference system [2]. This becomes clear when we consider the explicit form of the Hamiltonian $\hat{H}(\lambda)$ for a general N electron system in an external potential $v_{ext}(\mathbf{r}_i)$

$$\hat{H}(\lambda) = \sum_{i=1}^{N} \left[-\frac{1}{2}\nabla_i^2 + v^\lambda(\mathbf{r}_i) \right] + \sum_{i>j=1}^{N} \frac{\lambda}{|\mathbf{r}_i - \mathbf{r}_j|}, \tag{2.1.2}$$

where $v^\lambda(\mathbf{r}_i)$ denotes a not necessarily local one-particle potential [31], that depends on the coupling-strength parameter. From the Equations (2.1.1) and (2.1.2) it is clear that the electron-electron interaction is scaled by the parameter λ. Since the physical Hamiltonian is recovered for $\lambda = 1$ it is obvious that the one-particle potential corresponds just to the physical external potential $v^{\lambda=1}(i) = v_{ext}(\mathbf{r}_i)$. Switching off the interaction – i.e for $\lambda = 0$ – we are left with the reference Hamiltonian, which is just a summation over one-particle

Hamiltonians

$$\begin{aligned}\hat{H}_0 &= \sum_{i=1}^{N}\left[-\frac{1}{2}\nabla_i^2 + v^{\lambda=0}(\mathbf{r}_i)\right] \\ &= \sum_{i=1}^{N}\left[-\frac{1}{2}\nabla_i^2 + v_{ext}(\mathbf{r}_i) + v_{mf}(\mathbf{r}_i)\right].\end{aligned} \tag{2.1.3}$$

It includes the kinetic energy and the one-particle potential $v^{\lambda=0}(\mathbf{r}_i)$. Since the reference Hamiltonian describes an auxiliary system of non-interacting particles – like for example the Kohn-Sham system – the one-particle potential is split into the external potential and a mean-field potential $v_{mf}(i)$. Depending on the auxiliary systems, the mean-field potential might for example be the Hartree-Fock potential or, more commonly, the effective Kohn-Sham potential. Given the explicit form of the total Hamiltonian (2.1.2) and the one-body part $\hat{H}_0$ (2.1.3), we can express $\hat{H}_1$ in Eq. (2.1.1) as

$$\begin{aligned}\hat{H}_1(\lambda) &= \sum_{i>j=1}^{N}\frac{1}{|\mathbf{r}_i - \mathbf{r}_j|} + \frac{1}{\lambda}\left[v^{\lambda}(\mathbf{r}_i) - v^{\lambda=0}(\mathbf{r}_i)\right] \\ &= \sum_{i>j=1}^{N}\frac{1}{|\mathbf{r}_i - \mathbf{r}_j|} + \frac{1}{\lambda}\left[v^{\lambda}(\mathbf{r}_i) - v_{ext}(\mathbf{r}_i) - v_{mf}(i)\right].\end{aligned} \tag{2.1.4}$$

The Hamiltonian $\hat{H}_1(\lambda)$ includes the electron-electron interaction and ensures the adiabatic connection with the mean-field potential introduced in Eq. (2.1.3). Now that we have obtained explicit expressions for the two pieces forming our Hamiltonian, we can introduce normalized ground-state wave functions $\left|\Psi_0^{\lambda}\right\rangle$ that fulfill

$$\hat{H}(\lambda)\left|\Psi_0^{\lambda}\right\rangle = E^{\lambda}\left|\Psi_0^{\lambda}\right\rangle \tag{2.1.5}$$

for all possible values of the coupling-strength parameter λ. Since the ground-state wave functions are normalized, we can write down the ground-state expectation value of the λ-dependent system. In order to calculate the ground-state expectation value of the physical system we want to evaluate the derivative $\frac{\partial}{\partial\lambda}\left\langle\Psi_0^{\lambda}\middle|\hat{H}(\lambda)\middle|\Psi_0^{\lambda}\right\rangle$. Applying the Hellmann-Feynman theorem (1.2.9) and integrating both sides with respect to λ yields

$$\begin{aligned} E^{\lambda=1} &= E^{\lambda=0} + \int_0^1 d\lambda \left\langle \Psi_0^\lambda \middle| \frac{\partial}{\partial\lambda} \left(\hat{H}_0 + \lambda \hat{H}_1(\lambda) \right) \middle| \Psi_0^\lambda \right\rangle \\ &= E^{(0)} + \int_0^1 d\lambda \left\langle \Psi_0^\lambda \middle| \hat{H}_1(\lambda) + \lambda \frac{d\hat{H}_1(\lambda)}{d\lambda} \middle| \Psi_0^\lambda \right\rangle . \end{aligned} \tag{2.1.6}$$

In the above equation, we expressed the ground-state total energy E of the physical system (omitting the superscript $\lambda = 1$) as the ground-state energy of the non-interacting reference system plus a higher-order correction [31]. In this case the energy expectation value $E^{(0)} = \left\langle \Psi_0^{\lambda=0} \middle| \hat{H}_0 \middle| \Psi_0^{\lambda=0} \right\rangle$ can be interpreted as the zeroth-order energy to the total ground-state energy. Depending on the choice of the mean-field potential used in $\hat{H}_0$ the second term includes the missing correlation and exchange effects. Note that the path for the adiabatic connection in Eq. (2.1.6) is not unique [2, 31]. A linear connection yields a λ-independent $\hat{H}_1$ and thus the derivative in Eq. (2.1.6) drops out. This path is typically chosen in many-body perturbation theory (MBPT). In general, the electronic density of the system will change along the connection path, when only the interaction or the one-particle potential is modified. To derive the random-phase approximation within the DFT, the path is commonly chosen such that the electronic density is kept fixed at its physical value for all λ

$$n^\lambda(\mathbf{r}) = n^\lambda(\mathbf{r}) \,|_{\,\lambda=1} = n(\mathbf{r}). \tag{2.1.7}$$

This implies a non-trivial and not explicitly know λ-dependence of the two-body part of the Hamiltonian, since the one-particle potential ensures that the density is kept at its physical value. Therefore the physical system is connected with the Kohn-Sham auxiliary system and hence the mean-field potential corresponds to the Kohn-Sham effective potential. We can now further simplify the integrand in Eq. (2.1.6) by plugging in the explicit form of $\hat{H}_1(\lambda)$

$$\begin{aligned} E =& E^{(0)} + \int_0^1 d\lambda \left\langle \Psi_0^\lambda \middle| \frac{1}{2} \sum_{i\neq j=1}^{N} \frac{1}{|\mathbf{r}_i - \mathbf{r}_j|} + \frac{1}{\lambda} \sum_{i=1}^{N} \left[v^\lambda(\mathbf{r}_i) - v_{ext}(\mathbf{r}_i) - v_{mf}(i) \right] \middle| \Psi_0^\lambda \right\rangle \\ &+ \int_0^1 d\lambda \left\langle \Psi_0^\lambda \middle| -\frac{\lambda}{\lambda^2} \sum_{i=1}^{N} \left[v^\lambda(\mathbf{r}_i) - v_{ext}(\mathbf{r}_i) - v_{mf}(i) \right] + \sum_{i=1}^{N} \frac{d}{d\lambda} v^\lambda(\mathbf{r}_i) \middle| \Psi_0^\lambda \right\rangle \\ =& E^{(0)} + \int_0^1 d\lambda \left\langle \Psi_0^\lambda \middle| \frac{1}{2} \sum_{i\neq j=1}^{N} \frac{1}{|\mathbf{r}_i - \mathbf{r}_j|} \middle| \Psi_0^\lambda \right\rangle + \int_0^1 d\lambda \left\langle \Psi_0^\lambda \middle| \sum_{i=1}^{N} \frac{d}{d\lambda} v^\lambda(\mathbf{r}_i) \middle| \Psi_0^\lambda \right\rangle . \end{aligned} \tag{2.1.8}$$

We have split the integrand into the ground-state expectation value of the electron-electron interaction operator - a two-particle operator - and the expectation value of a one-particle operator. Introducing one- and two-particle density operators we can rewrite the corresponding operators as [32]

$$\begin{aligned}\sum_{i=1}^{N}\frac{d}{d\lambda}v^{\lambda}(\mathbf{r}_i) &= \int d\mathbf{r}\hat{n}(\mathbf{r})\frac{d}{d\lambda}v^{\lambda}(\mathbf{r}) \\ \sum_{i\neq j=1}^{N}\frac{1}{|\mathbf{r}_i-\mathbf{r}_j|} &= \int\int d\mathbf{r}d\mathbf{r}'\frac{\hat{n}(\mathbf{r},\mathbf{r}')}{|\mathbf{r}-\mathbf{r}'|}.\end{aligned} \tag{2.1.9}$$

Here $\hat{n}(\mathbf{r})$ and $\hat{n}(\mathbf{r},\mathbf{r}')$ denote the one- and two-body density operators respectively. Recall that we chose the connection such that the density is fixed at the physical one for all λ. This implies that the ground-state expectation value of the density operator yields the physical electronic density $\left\langle\Psi_0^{\lambda}\middle|\hat{n}(\mathbf{r})\middle|\Psi_0^{\lambda}\right\rangle = n(\mathbf{r})$ for any λ [31]. Using this we can evaluate the integrand of the second term in Eq. (2.1.8) and perform the λ integration

$$\begin{aligned}\int_0^1 d\lambda\left\langle\Psi_0^{\lambda}\middle|\sum_{i=1}^{N}\frac{d}{d\lambda}v^{\lambda}(\mathbf{r}_i)\middle|\Psi_0^{\lambda}\right\rangle &= \int d\mathbf{r}n(\mathbf{r})\left[v^{\lambda=1}(\mathbf{r})-v^{\lambda=0}(\mathbf{r})\right] \\ &= -\int d\mathbf{r}n(\mathbf{r})v_{mf}(\mathbf{r}).\end{aligned} \tag{2.1.10}$$

In the last step we used the fact that the $v^{\lambda=1} = v_{ext}$ and $v^{\lambda=0} = v_{ext} + v_{mf}$. The expression we found describes the classical potential energy of an electronic density interacting with a mean-field potential. Since we keep the electronic density fixed at its physical value, the zeroth-order contribution to the total ground-state energy is just the Kohn-Sham ground-state energy. Expanding $E^{(0)}$ using $\left|\Psi_0^{\lambda=0}\right\rangle = |\Phi_0\rangle$, where $|\Phi_0\rangle$ is the Kohn-Sham wave function, yields

$$\begin{aligned}E^{(0)} &= \left\langle\Phi_0\middle|\sum_{i=1}^{N}\left[-\frac{1}{2}\nabla_i^2+v^{\lambda=0}(\mathbf{r}_i)\right]\middle|\Phi_0\right\rangle \\ &= T_s[n]+\int d\mathbf{r}n(\mathbf{r})v^{\lambda=0}(\mathbf{r}) \\ &= T_s[n]+\int d\mathbf{r}n(\mathbf{r})\left[v_{ext}(\mathbf{r})+v_{mf}(\mathbf{r})\right].\end{aligned} \tag{2.1.11}$$

Here we rewrote the one-particle potential $v^{\lambda=0}$ as the external potential plus the mean-field potential. The zeroth-order energy contains the non-interacting kinetic energy $T_s[n]$, the

potential energy associated with the external potential and the potential energy arising from the electronic density interacting with the mean-field potential. Combining Eqs. (2.1.8),(2.1.10) and (2.1.11) we find that the terms describing the mean-field energy cancel each other. Thus we are left with the following expression for the total ground-state energy

$$E = T_s[n] + \int d^3r n(\mathbf{r}) v_{ext}(\mathbf{r}) + \int d\lambda \int\int d\mathbf{r} d\mathbf{r}' \left\langle \Psi_0^\lambda \middle| \frac{\hat{n}(\mathbf{r},\mathbf{r}')}{|\mathbf{r}-\mathbf{r}'|} \middle| \Psi_0^\lambda \right\rangle . \tag{2.1.12}$$

The first and second terms correspond to the non-interacting kinetic energy and the physical external potential energy respectively. Note that the mean-field potential no longer appears. The full many-body complexity is contained within the third term. The electron-electron interaction is expressed as the coupling strength integral over all ground-state expectation values of the Coulomb operator. Note that the interacting part of the kinetic energy contributes to the correlation energy and is thus included in the third term. The next step is to rewrite the pair-density in terms of one-body operators to evaluate the expectation value in the third term. Therefore we start with the definition of the two-body density operator in second quantization and use the fermionic anti-commutation relations to rewrite it in terms of one-body density operators $\hat{n}(\mathbf{r}) = \hat{\psi}^\dagger(\mathbf{r})\hat{\psi}(\mathbf{r})$

$$\begin{aligned}
\hat{n}(\mathbf{r},\mathbf{r}') =& \frac{1}{2}\hat{\psi}^\dagger(\mathbf{r})\hat{\psi}^\dagger(\mathbf{r}')\hat{\psi}(\mathbf{r}')\hat{\psi}(\mathbf{r}) \\
=& \frac{1}{2}\hat{\psi}^\dagger(\mathbf{r})\hat{\psi}(\mathbf{r})\hat{\psi}^\dagger(\mathbf{r}')\hat{\psi}(\mathbf{r}') - \frac{1}{2}\delta(\mathbf{r}-\mathbf{r}')\hat{\psi}^\dagger(\mathbf{r})\hat{\psi}(\mathbf{r}) \\
=& \frac{1}{2}\hat{n}(\mathbf{r})\hat{n}(\mathbf{r}') - \frac{1}{2}\delta(\mathbf{r}-\mathbf{r}')\hat{n}(\mathbf{r}),
\end{aligned} \tag{2.1.13}$$

where $\hat{\psi}(\mathbf{r})$ and their adjoints denote the electron field operators [32]. Introducing the density fluctuation operator $\Delta\hat{n}(\mathbf{r}) = \hat{n}(\mathbf{r}) - n(\mathbf{r})$, where we subtract its expectation value $n(\mathbf{r})$ from the density operator $\hat{n}(\mathbf{r})$, we rewrite the first term in the above equation

$$\hat{n}(\mathbf{r},\mathbf{r}') = \frac{1}{2}\left[\Delta\hat{n}(\mathbf{r})\Delta\hat{n}(\mathbf{r}') - n(\mathbf{r})\Delta\hat{n}(\mathbf{r}') - \Delta\hat{n}(\mathbf{r})n(\mathbf{r}') + n(\mathbf{r})n(\mathbf{r}') - \delta(\mathbf{r}-\mathbf{r}')\hat{n}(r)\right]. \tag{2.1.14}$$

We can now insert Eq. (2.1.14) back into Eq. (2.1.12). Since the ground-state expectation value of the density-fluctuation operator is zero, the second and third terms do not contribute and we are left with

$$\begin{aligned} E =& T_s[n] + \int d\mathbf{r} n(\mathbf{r}) v_{ext}(\mathbf{r}) + \frac{1}{2}\int\int d\mathbf{r} d\mathbf{r}' \frac{n(\mathbf{r})n(\mathbf{r}')}{|\mathbf{r}-\mathbf{r}'|} + \\ &+ \frac{1}{2}\int_0^1 d\lambda \int\int d\mathbf{r} d\mathbf{r}' \left\langle \Psi_0^\lambda \middle| \frac{\Delta\hat{n}(\mathbf{r})\Delta\hat{n}(\mathbf{r}') - \delta(\mathbf{r}-\mathbf{r}')\hat{n}(\mathbf{r})}{|\mathbf{r}-\mathbf{r}'|} \middle| \Psi_0^\lambda \right\rangle . \end{aligned} \tag{2.1.15}$$

Comparing the expression of the total ground-state energy we obtained with the universal energy functional (1.1.6) within the Kohn-Sham method, we have already noted that the first two terms are the non-interacting kinetic energy and the external potential energy functional $E_{ext}[n]$. Furthermore, we can identify the second to last term as the Hartree energy functional $E_H[n]$. We have isolated the classical electrostatic interaction energy from the total interaction energy. Therefore the last term is the remaining non-classical contribution to the interaction energy - the exchange and correlation energy. The expression we found for the exchange and correlation energy is exact but involves an integral over all ground-state expectation values and hence the evaluation of the Ψ_0^λ. The goal is to somehow further simplify the integrand, isolate the correlation energy and find a systematic approximation for it.

Comparing the expression (2.1.15), where we isolated the exchange-correlation energy, with the adiabatic connection formula (1.2.17) we can define the exchange-correlation hole as

$$n_{xc}^\lambda(\mathbf{r}', \mathbf{r}) = \frac{\left\langle \Psi_0^\lambda \middle| \Delta\hat{n}(\mathbf{r})\Delta\hat{n}(\mathbf{r}') \middle| \Psi_0^\lambda \right\rangle}{n(\mathbf{r})} - \delta(\mathbf{r}-\mathbf{r}') \tag{2.1.16}$$

and write the exchange-correlation energy as

$$E_{xc}[n] = \frac{1}{2}\int_0^1 d\lambda \int\int d\mathbf{r} d\mathbf{r}' \frac{n(\mathbf{r}) n_{xc}^\lambda(\mathbf{r}', \mathbf{r})}{|\mathbf{r}-\mathbf{r}'|}. \tag{2.1.17}$$

Thus we have once more discovered the adiabatic connection formula (1.2.17) for the exchange-correlation energy. As we expressed the pair-density operator arising in the electron-electron interaction operator in terms of one-body density operators, we found an expression for the exchange-correlation hole. It depends on density-fluctuations and therefore it is obvious to link it to the density-density correlation function. This is the topic of the next section.

2.1.1 The fluctuation-dissipation theorem

In this section, we use the fluctuation-dissipation theorem to further simplify the exchange-correlation hole, for which we found an expression at the end of the last section. The theorem was proven by Callen and Welton [33] in 1951 and relates the dissipation of a system affected by an external perturbation and the spontaneous internal fluctuations in the absence of the perturbation [31, 34].
Looking at the expression we found for the exchange-correlation hole (2.1.16) we find that it is closely related to the density-density correlation function $\langle \hat{n}(\mathbf{r})\hat{n}(\mathbf{r}')\rangle_0$. Therefore we link the exchange-correlation hole to the response properties of the system.

$$\left\langle \Psi_0^\lambda \middle| \Delta\hat{n}(\mathbf{r})\Delta\hat{n}(\mathbf{r}') \middle| \Psi_0^\lambda \right\rangle = -\int_0^\infty \frac{d\omega}{\pi} \operatorname{Im}\chi^\lambda(\omega, \mathbf{r}, \mathbf{r}'). \tag{2.1.18}$$

This is a consequence of the zero-temperature fluctuation-dissipation theorem [31, 32, 35]. Note that the linear density-density response function depends on the coupling strength parameter. Due to the analytic structure of χ and the fact that it is real-valued along the imaginary axis, the frequency integration can be performed along the imaginary axis [31] using a Wick rotation [36]. Inserting Eq. (2.1.18) back into Eq. (2.1.17) we obtain

$$E_{xc}[n] = \frac{1}{2\pi}\int_0^1 d\lambda \int\int d\mathbf{r}d\mathbf{r}' \frac{1}{|\mathbf{r}-\mathbf{r}'|}\left[-\int_0^\infty d\omega \chi^\lambda(\mathbf{r}, \mathbf{r}', i\omega) - \delta(\mathbf{r}-\mathbf{r}')n(\mathbf{r})\right], \tag{2.1.19}$$

where we perform the frequency integration along the imaginary axis as stated above. We found an expression for the exchange-correlation energy in terms of the frequency-dependent linear density response function. The latter describes the response of the one-electron density and can be obtained from the time-dependent density functional theory [37]. Furthermore, relying on time dependent density functional theory, it fulfills the following Dyson equation [35, 38]

$$\begin{aligned}\chi^\lambda(\mathbf{r}, \mathbf{r}', i\omega) = &\chi^0(\mathbf{r}, \mathbf{r}', i\omega) + \int d\mathbf{r}_1 d\mathbf{r}_2 \chi^0(\mathbf{r}, \mathbf{r}_1, i\omega) \\ &\times \left(\frac{\lambda}{|\mathbf{r}_1 - \mathbf{r}_2|} + f_{xc}^\lambda(\mathbf{r}_1, \mathbf{r}_2, \omega)\right)\chi^\lambda(\mathbf{r}_2, \mathbf{r}', i\omega),\end{aligned} \tag{2.1.20}$$

where $\chi^0(\mathbf{r}, \mathbf{r}', i\omega)$ is the independent particle response function of the auxiliary Kohn-Sham system and f_{xc} is the exchange-correlation kernel at coupling strength λ. The Eq. (2.1.20) is exact but the form of the exchange-correlation kernel is unknown. The Eqs. (2.1.19) and (2.1.20) define the exchange-correlation energy in the fluctuation-

dissipation theorem density functional theory framework. It differs from conventional DFT which relies on approximations of the exchange-correlation energy functional. Possible functionals are found within the LDA, GGA or with hybrid approximations as discussed in section 1.1. Because it is computationally more demanding to compute the full response function χ^λ than performing a normal DFT calculation, the FDT-DFT formalism might seem unnecessarily complicated. Nevertheless, it yields useful results even in the simplest approximation $f_{xc}^\lambda = 0$ – the random-phase approximation. In conventional DFT setting the exchange-correlation energy functional $E_{xc}[n] = 0$ corresponds to the Hartree approximation, which includes neither exchange nor correlation. Here exchange and even some correlation effects are included.

2.2 The random-phase approximation

As mentioned at the end of the last section, we are now close to the random-phase approximation. We discussed the ACFD theorem and found a formally exact expression for the correlation energy of an interacting system. The random-phase approximation arises as a natural zero-order approximation of the correlation energy within this formalism. An alternative derivation using many-body perturbation theory (MBPT) is also discussed below. This will highlight the close connection of the RPA to the GW framework and will yield a diagrammatic representation of the correlation energy within the RPA. Finally, the RPA is compared to conventional exchange-correlation functionals. Its benefits and drawbacks are highlighted while also some improvements are discussed.

2.2.1 RPA derived from ACFD theory

Recall that the exact form of the exchange-correlation kernel f_{xc} as a density functional is unknown. The simplest possible "approximation" for the exchange-correlation kernel is the so-called random-phase approximation (RPA). It simply sets it $f_{xc}^{RPA} = 0$, and therefore only the Hartree kernel remains. The resulting Dyson-type equation

$$\chi_{RPA}^\lambda(\mathbf{r}, \mathbf{r}', i\omega) = \chi^0(\mathbf{r}, \mathbf{r}', i\omega) + \lambda \int d\mathbf{r}_1 d\mathbf{r}_2 \frac{\chi^0(\mathbf{r}, \mathbf{r}_1, i\omega)\chi_{RPA}^\lambda(\mathbf{r}_2, \mathbf{r}', i\omega)}{|\mathbf{r}_1 - \mathbf{r}_2|} \tag{2.2.1}$$

can be solved for χ_{RPA}^λ [30]. As mentioned before χ^0 denotes the independent particle response function of the Kohn-Sham system, which is given in its spectral representation in terms of the KS spin-orbitals $\phi_{i,\sigma}(\mathbf{r})$ and their energies $\epsilon_{i,\sigma}$ [31, 39, 40]

$$\chi^0(\mathbf{r},\mathbf{r}',i\omega) = \sum_{i,j}(f_i - f_j)\,\frac{\phi_i^*(\mathbf{r})\phi_j(\mathbf{r})\phi_j^*(\mathbf{r}')\phi_i(\mathbf{r}')}{\epsilon_i - \epsilon_j - i\omega}, \tag{2.2.2}$$

where the sums run over all occupied and unoccupied orbitals. The f_i denote the Fermi occupations of the respective orbitals. This term ensures that there is only a contribution if one orbital is occupied and the other is empty. Combining the Eqs. (2.2.2), (2.2.1) and (2.1.19) we find the exchange-correlation energy within the random-phase approximation. It can be separated into an exact (KS) exchange E_x^{EX} and an RPA correlation term E_c^{RPA}

$$E_{xc}^{RPA} = E_x^{EX} + E_c^{RPA}, \tag{2.2.3}$$

where

$$\begin{aligned} E_x^{EX} =& \frac{1}{2\pi}\int\int d\mathbf{r}d\mathbf{r}'\frac{1}{|\mathbf{r}-\mathbf{r}'|}\Big[-\int d\omega\chi^0(\mathbf{r},\mathbf{r}',i\omega) - \delta(\mathbf{r}-\mathbf{r}')n(\mathbf{r})\Big] \\ =& -\frac{1}{2}\sum_\sigma\sum_{i,j}^{occ}\int\int d\mathbf{r}d\mathbf{r}'\frac{\phi_{i,\sigma}^*(\mathbf{r})\phi_{j,\sigma}(\mathbf{r})\phi_{j,\sigma}^*(\mathbf{r}')\phi_{i,\sigma}(\mathbf{r}')}{|\mathbf{r}-\mathbf{r}'|} \end{aligned} \tag{2.2.4}$$

and

$$\begin{aligned} E_c^{RPA} =& -\frac{1}{2\pi}\int\int d\mathbf{r}d\mathbf{r}'\frac{1}{|\mathbf{r}-\mathbf{r}'|}\int_0^\infty d\omega\left[\int_0^1 d\lambda\chi_{RPA}^\lambda(\mathbf{r},\mathbf{r}',i\omega) - \chi^0(\mathbf{r},\mathbf{r}',i\omega)\right] \\ =& \frac{1}{2\pi}\int_0^\infty d\omega\,\mathrm{Tr}\Big[ln(1-\chi^0(i\omega)v) + \chi^0(i\omega)v\Big]. \end{aligned} \tag{2.2.5}$$

Having a look at the final equation for the exact exchange energy, we see that it corresponds to the exchange energy we find in Hartree-Fock theory, where the HF orbitals have been changed to the KS orbitals. Because the exchange energy arises from the anti-symmetry of the wave function, there are only contributions, if the particles' spins are aligned.
Looking at the correlation energy: in Eq. (2.2.5) the Coulomb kernel is abbreviated $v(\mathbf{r},\mathbf{r}') = 1/|\mathbf{r}-\mathbf{r}'|$ and the double spatial integral is shortened using the following convention [31]

$$\mathrm{Tr}[AB] = \int\int d\mathbf{r}\mathbf{r}'A(\mathbf{r},\mathbf{r}')B(\mathbf{r},\mathbf{r}'). \tag{2.2.6}$$

Once the independent particle response function χ^0 has been computed using the occupied and all the unoccupied orbitals it is straightforward to evaluate the RPA correlation energy. The random-phase approximation poses a systematic approach to improve on the

conventional exchange-correlation functionals. Its advantage compared to GGA functionals is that it treats the exchange energy and parts of the correlation energy exactly. While hybrid functionals try to incorporate a fraction of exact exchange, is it always a bit empirical how those are constructed. The RPA is a systematic approach to approximate the correlation energy, while fully accounting for exact exchange. Note that conventional DFT correlation functionals can not be combined with exact exchange.

2.2.2 RPA derived from MBPT

We have derived the random-phase approximation for the correlation energy in the ACFD formalism, where it arose at a natural first-order approximation. However, the correlation energy can also be discussed in the context of many-body perturbation theory [3, 31, 40]. Starting from Eq. (2.1.6), instead of keeping the density fixed along the connection a linear path is chosen, i.e. $v^\lambda(\mathbf{r}_i) = v_{ext}(\mathbf{r}_i) + (1-\lambda)v_{mf}(i)$. Therefore $\hat{H}_1(\lambda)$ in Eq. (2.1.4) is λ-independent and thus the interacting ground-state energy takes a particularly simple form

$$E = E^{(0)} + \int_0^1 d\lambda \left\langle \Psi_0^\lambda \middle| \hat{H}_1 \middle| \Psi_0^\lambda \right\rangle . \tag{2.2.7}$$

A Taylor expansion of $|\Psi_0^\lambda\rangle$ and a coupling-strength integration leads to an order-by-order expansion of the total ground-state energy. Up to the first-order, this approach equals the Hartree-Fock energy. The second-order term represents the second-order Møller–Plesset (MP2) energy, where the first correlation corrections appear. The expansion of Eq. (2.2.7) up to second-order reads

$$E = \left\langle \Phi_0 \middle| \hat{H}_0 \middle| \Phi_0 \right\rangle + \left\langle \Phi_0 \middle| \hat{H}_1 \middle| \Phi_0 \right\rangle + \sum_{n \neq 0} \frac{\left\langle \Phi_0 \middle| \hat{H}_1 \middle| \Phi_n \right\rangle \left\langle \Phi_n \middle| \hat{H}_1 \middle| \Phi_0 \right\rangle}{E^{(0)} - E_n^{(0)}} + ..., \tag{2.2.8}$$

where $|\Phi_0\rangle = |\Psi_0^{\lambda=0}\rangle$ is the ground-state wave function of $\hat{H}_0$ and $|\Phi_n\rangle$ are excited determinants of the reference Hamiltonian with energies $E_n^{(0)}$. Excited states are denoted by how they differ from a given reference state, which is usually chosen to be the ground-state wave function. Take for example the singly-excited state Φ_i^a: the i-th single-particle state of the ground-state determinant is excited to the a-th unoccupied state. Note that the sum appearing in the second-order term runs over all possible excited determinants. Since $\hat{H}_1$ contains at most a two-particle operator the sum can be restricted to singly- and doubly-excited states $|\Phi_i^a\rangle$ and $|\Phi_{ij}^{ab}\rangle$ respectively. The reason being that the determinants are built out of orthonormal single-particle orbitals, which are eigenstates of the unperturbed

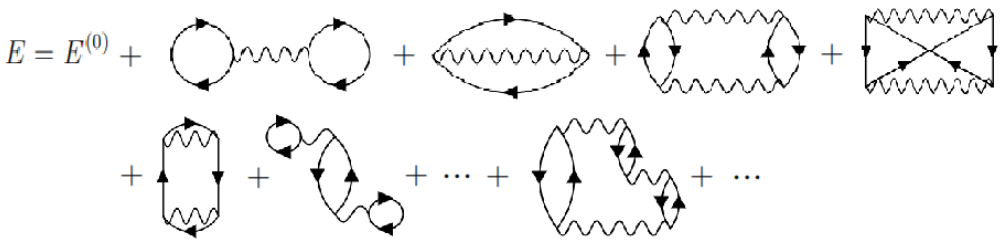

Figure 2.1: Diagrammatic representation of the first few terms in Eq. (2.2.8). The $E^{(0)}$ contains the kinetic and external potential energy. The first four diagrams from left to right correspond to the Hartree-, exchange-, direct- and indirect MP2 energy. Solid lines correspond to electrons (up-going propagator) and holes (down-going propagator), while the wiggly lines represent the bare Coulomb interaction.

Hamiltonian. Acting with a two-particle operator at a thirdly- or higher-excited state would leave at least one excited orbital unpaired with those of the ground-state determinant setting the whole term to zero. Furthermore, Brillouin's theorem [3] states that singly-excited determinants do not directly interact with a Hartree-Fock ground-state. This means $\langle\Phi_0|\hat{H} - \hat{H}_0|\Phi_n\rangle = 0$, where the first term vanishes due to Brillouin's theorem and the second because the single-particle orbitals are eigenstates of $\hat{H}_0$. Therefore the sum in the second-order term runs only over doubly-excited states.

The terms in Eq. (2.2.8) are usually evaluated diagrammatically using Feynman diagrams as seen in Fig. (2.1). For more details on how to evaluate these diagrams see e.g. the book by Mattuck [41]. The ground-state energy is built up as a sum over all linked diagrams which start and end in the many-body ground-state. These diagrams get complicated quickly and it is impractical to sum all of them to infinite order. Therefore one can either truncate the diagrammatic expansion at a certain point or include only important subsets of the higher-order diagrams. For example to obtain the Hartree-Fock energy the expansion is truncated at the first-order exchange diagram (see Fig. (2.1)), while MP2 also includes the first two second-order diagrams. An example for a subset of diagrams is a partial sum over all second- and higher-order diagrams with closed fermion loops [41]. Including these so-called bubble diagrams yield the random-phase approximation for the correlation energy. While in the last section the RPA was derived from DFT we now found it in the context of MBPT. This allows us to obtain a diagrammatic representation of the RPA correlation energy.

These diagrams are usually evaluated using Green's function theory, which describes how a particle propagates in the system [12, 41]. A Green's function describes how an additional electron (or hole) at $\{\mathbf{r}, t\}$ will propagate through the system and how likely

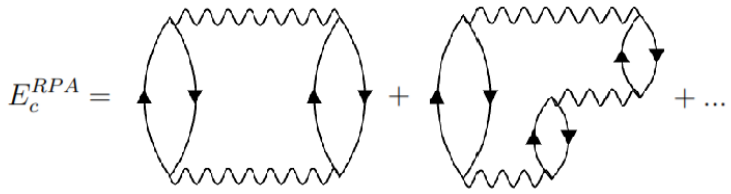

Figure 2.2: Second- and third-order bubble diagrams of the RPA correlation energy. Solid lines correspond to electrons (up-going propagator) and holes (down-going propagator), while the wiggly lines represent the bare Coulomb interaction.

it is to encounter it at $\{\mathbf{r}', t'\}$. Therefore it is commonly called a propagator. In the last section, we obtained the random-phase approximation to the density response function χ by neglecting the exchange-correlation kernel. In the context of the MBPT, we obtain the RPA by approximating the response to the independent-particle potential as [12]

$$\chi^0(1,2) = -iG^0(1,2)G^0(2,1), \tag{2.2.9}$$

where G^0 is the independent particle Green's function. Diagrammatically this corresponds to a closed electron-hole bubble. Thus the Dyson-type equation for the RPA density response function (2.2.1) yields a sum of bubble diagrams. Note that the above equation corresponds to a self-consistent GW calculation if instead of G^0 the interacting Green's function G is used. This shows the close connection between the random-phase and GW approximation. The latter solves a set of equations (Hedin's equations) self-consistently [12]

$$\begin{aligned} G(1,2) =& G^0(1,2) + G^0(1,\bar{3})\Sigma(\bar{3},\bar{4})G(\bar{4},2) \\ \chi(1,2) =& -iG(1,2)G(2,1) \\ W(1,2) =& v(1,2) + v(1,\bar{3})\chi(\bar{3},\bar{4})W(\bar{4},2) \\ \Sigma(1,2) =& iG(1,2)W(2,1). \end{aligned} \tag{2.2.10}$$

The first equation is the Dyson equation for the Green's function in terms of the non-interacting Green's function and the so-called self-energy Σ. The latter is defined as the sum of all proper amputated Feynman diagrams. This means that the diagrams can not be split into two by cutting any internal electron propagator and in- and out-going propagators are removed. Furthermore, χ is the irreducible polarizability and W is the screened Coulomb interaction, where v is the Coulomb interaction. The Dyson-type equation for the screened interaction reflects the self-consistent response of a system

to external and induced classical potentials [12]. Because these equations need to be solved self-consistently an initial guess for the Green's functions is required. Usually, the independent-particle Green's function calculated from an underlying HF or DFT calculation is used. Thus the first GW self-consistency cycle corresponds to the RPA [42] and the RPA self-energy can be written as $\Sigma^{RPA}(1,2) = G^0(1,2)W^0(2,1)$.
Besides its close connection to the GW method McLachlan and Ball [43] pointed out that, when combined with the exact exchange, the RPA is equivalent to time-dependent Hartree-Fock theory, if the independent-particle Green's functions in Eq. (2.2.9) are evaluated with Hartree-Fock single-particle orbitals. Furthermore Scuseria [44] showed the relation to coupled cluster theory.

2.2.3 Performance and improvements of RPA

In this section, the advantages and drawbacks of the random-phase approximation will be discussed. We will start with one of its main limitations, namely its computational cost. As it involves the calculation of the independent particle response function a summation over all occupied and unoccupied states needs to be performed. To obtain converged results, larger basis sets are needed [40]. Plane-wave implementations of the RPA commonly scale with $O(N^4)$ with the system size, however, a cubic scaling algorithm has been proposed by Kaltak and co-workers [45] and implemented in VASP.
Conventional exchange-correlation functionals as LDA and GGA have some serious limitations one of which is self-interaction. This arises because the approximate exchange does not completely cancel the self-interaction present in the Hartree energy. This could, in principle, be removed by combining LDA or GGA correlation energies with the exact exchange energy. Unfortunately, this generally leads to worse results, because those functionals heavily rely on some error cancellation between the exchange and correlation energy. Since this error cancellation leaves the exchange-correlation hole in these conventional functionals relatively short-ranged they also miss an accurate long-range description of the correlation energy [46, 47]. Thus, while covalent, metallic and ionic bonding are described reasonably, van der Waals forces are ill-described by the conventional functionals [45].
The random-phase approximation can naturally be combined with the exact exchange functional as it is the first-order approximation of the correlation energy. Therefore the self-interaction error is avoided. Furthermore, the RPA is known to describe the long-range interactions well but it fails to accurately describe short-range correlations [47]. This is due to the incorrect short-range behavior of the RPA response functions, where electrons only respond to the averaged density fluctuations. This leads to a self-response of an

electron to its density fluctuations [48]. Furthermore, the selective summation of the diagrams, namely only those with closed electron-hole loops as seen in Fig. (2.2), leads to an error. Exchange-like diagrams, like the second-order exchange MP2 diagram in Fig. (2.1 are not included in the RPA. This leads to a negative pair-correlation function of the uniform electron gas (UEG) for small distances between electrons [31]. Therefor a semi-local correction term has been proposed [31, 46, 47], which cancels the short-range correlation error within the RPA

$$E_{c,s.r.}^{LDA} = E_c^{LDA} - E_c^{LDA-RPA} \tag{2.2.11}$$

Here E_c^{LDA} is the correlation energy found within the LDA and $E_c^{LDA-RPA}$ is the part of the RPA correlation energy also treated within LDA. Thus added to the RPA correlation energy the correction 2.2.11 treats the short-range correlation energy within LDA or alternatively GGA. This method is referred to as RPA+. It yields improved total correlation energies but does not significantly improve energy differences [31,38,47]. Thus, the standard RPA is a promising method to obtain accurate correlation energy differences but it overestimates absolute correlation energies.

Another logical step to go beyond the standard RPA is to improve the interacting density response function. This can be achieved by employing a different approximation for the exchange-correlation kernel appearing in the corresponding Dyson-type equation (2.1.20). One possibility is to use the exchange kernel f_{xc}^{RPA+X} from time-dependent DFT [48, 49] instead of applying the random-phase approximation $f_{xc}^{RPA} = 0$.

Currently, RPA calculations are done mostly in a post-processing manner. This means that the KS orbitals from a previous DFT calculation are used for a one-shot RPA calculation. Therefore the results may depend on the input orbitals used. A self-consistent RPA approach can be formulated but is computationally still challenging. For the future, this is a promising avenue to improve on the current RPA implementations.

Chapter 3

Natural orbitals

In the last two chapters, we have discussed that conventional mean-field methods like DFT or HF theory miss out on some important aspects of the electron correlations. To include those effects in our calculations, higher hierarchy methods need to be applied. We discussed the random-phase approximation as a post-Kohn-Sham method in the last chapter. Besides RPA, there are plenty of other methods, which take correlation effects into account in an approximate manner. Some of them were already mentioned like coupled-cluster or Møller–Plesset perturbation theory (MPn) but there are others. For example configuration interaction (CI), which is conceptually very simple but unfortunately computationally intractable for more than 10 electrons, as it scales combinatorically with respect to the number of orbitals M and electrons N, e.g. $\binom{M}{N}$. As we have seen in the case of the RPA, an underlying calculation at the mean-field level (for example DFT or HF) can provide a single-particle basis for the higher hierarchy methods. All these methods have in common that, to treat electron correlations, virtual states are needed. Those are per definition the unoccupied eigenstates of the underlying mean-field calculations. To obtain accurate correlation energies a sufficient number of virtual states, spanning the relevant unoccupied subspace, need to be included in the calculation.
In the limit of a complete basis, the correlation energy becomes exact in the limit of the applied approximation. Therefore, we will refer to this correlation energy as the complete basis set limit. Unfortunately, we can only handle finite basis sets, thus the number of virtual states included in the calculation must be truncated at some point. This restricts the correlation energy only to a subspace of virtual states. Summarized, there are two separate approximations at play here. One is the method used to approximate the correlation energy and the other one relates to a truncation of the basis set. Truncating the basis set will yield just an approximation to the complete basis set limit.

Up to now, we were only concerned with Slater determinants but what is the form of the real interacting wave function? The answer is remarkably simple and I want to begin this chapter by discussing this question. It will guide us to the configuration interaction method - a post-Hartree-Fock method - which we will briefly discuss. The configuration interaction will motivate the introduction of so-called natural orbitals, which will be the topic of the remainder of this chapter.

3.1 The interacting ground-state wave function

In Hartree-Fock theory, the interacting many-body wave-function is approximated to be a Slater-determinant. We denote the HF ground-state wave function by Φ_0. It is built out of the N lowest single-particle orbitals, which correspond to the occupied states of the system. They are obtained by solving the self-consistent HF equations in a finite basis set [3]. For a complete basis set, the HF ground-state wave function corresponds to the HF limit. This is the best possible approximation to the interacting ground-state wave function in the restricted subspace of single determinants. But what does the interacting ground-state wave function look like?
Suppose we have a complete basis of some functions $\{\phi_i(x)\}$. Then we can expand any single-variable function using this basis set as

$$\Psi(x_1) = \sum_i a_i \phi_i(x_1). \tag{3.1.1}$$

This is straightforward, but we can continue and expand any two-variable function using the same basis set if we think of the expansion coefficients as being functions of x_2

$$\Psi(x_1, x_2) = \sum_i a(x_2)\phi_i(x_1). \tag{3.1.2}$$

Therefore, we can expand the coefficients analogous to Eq. (3.1.1) using the initial basis. This yields

$$\Psi(x_1, x_2) = \sum_{i,j} b_{ij}\phi_i(x_1)\phi_j(x_2). \tag{3.1.3}$$

Since we are interested in wave functions we require our function Ψ to be antisymmetric, i.e $\Psi(x_1, x_2) = -\Psi(x_2, x_1)$. Thus the expansion coefficients in Eq. (3.1.3) are antisymmetric too. We write

$$\begin{aligned}\Psi(x_1, x_2) =& \sum_{i<j} b_{ij} \left[\phi_i(x_1)\phi_j(x_2) - \phi_j(x_1)\phi_i(x_2)\right] \\ =& \sum_{i<j} 2^{1/2} b_{ij} \left|\phi_i\phi_j\right\rangle ,\end{aligned} \tag{3.1.4}$$

where we introduced the notation $|\phi_i\phi_j\rangle$ for a normalized Slater determinant. The sum in the above equation runs overall 2-particle Slater-determinants formed from the complete set of single-variable functions $\{\phi_i(x_1)\}$. Thus we have shown that an arbitrary antisymmetric two-variable (wave) function can be expanded using all 2-particle Slater-determinants, built from the complete set of single-particle orbitals. This can easily be extended to antisymmetric functions with N variables [3]. We conclude that the interacting ground-state wave function of a N-particle system is given as a linear combination of all possible N-particle determinants built from a complete set of single-particle orbitals. Thus the interacting ground-state wave function can be written in terms of a reference determinant $|\Phi_0\rangle$ (e.g. HF wave function) and its excited determinants

$$\begin{aligned}\left|\Psi_0\right\rangle =& c_0 \left|\Phi_0\right\rangle + \left(\frac{1}{1!}\right)^2 \sum_{ar} c_a^r \left|\Phi_a^r\right\rangle + \left(\frac{1}{2!}\right)^2 \sum_{abrs} c_{ab}^{rs} \left|\Phi_{ab}^{rs}\right\rangle \\ &+ \left(\frac{1}{3!}\right)^2 \sum_{\substack{\text{abc}\\ \text{rst}}} c_{abc}^{rst} \left|\Phi_{abc}^{rst}\right\rangle + \left(\frac{1}{4!}\right)^2 \sum_{\substack{\text{abcd}\\ \text{rstu}}} c_{abcd}^{rstu} \left|\Phi_{abcd}^{rstu}\right\rangle + ...,\end{aligned} \tag{3.1.5}$$

where the factors $(1/n!)^2$ ensures that each excited determinant is only counted once. Assume we have a set of $2M$ spin-orbitals from an underlying mean-field calculation, then we can construct $\binom{2M}{N}$ distinct N-particle determinants. Diagonalizing the Hamiltonian in the basis of this N-electron determinants solves the eigenvalue problem in the N-electron subspace spanned by the set of determinants. Equivalently one can use the variational principle to find the minimizing coefficients of the Eq. (3.1.5). In the limit of a complete set of N-particle Slater-determinants the resulting ground-state wave function would be exact. This insight is the foundation of the full configuration interaction (FCI), but obviously the number of coefficients becomes intractable very quickly (imagine $\binom{100}{10}$).

3.2 Full configuration interaction

The configuration interaction is a post-Hartree-Fock method to calculate the ground-state energy of an interacting N-particle system. In the following it is discussed qualitatively

to motivate the introduction of natural orbitals. For a more detailed review see e.g. [3]. The idea of the configuration interaction is to diagonalize the Hamiltonian in the basis of N-particle Slater-determinants formed from the spin-orbitals of an underlying HF calculation. Each determinant corresponds to a unique configuration of the orbitals, hence the name configuration interaction. The correlation energy is defined as the difference between the FCI ground-state energy and the HF energy, evaluated with the same orbitals. In the limit of a complete one-electron basis, the FCI correlation energy is exact. The method is a useful benchmark because the correlation energy is exact within the subspace spanned by the one-particle orbitals. This means the full CI correlation energy is the best one can do in a given subspace and thus other methods might be compared to how they perform with the same basis set.
Following the procedure of the variational method, i.e. multiplying $\hat{H}|\Psi_0\rangle = \epsilon_0|\Psi_0\rangle$ from left with all the determinants $\langle\Psi_0|$, $\langle\Phi_a^r|$, $\langle\Phi_{ab}^{rs}|$,... one ends up with a hierarchy of coupled equations, which need to be solved simultaneously. The more excited determinants are included in the expansion of the ground-state wave function, the more equations one has to solve. In other words, the Hamiltonian matrix in the basis of the N-particle determinants one has to diagonalize is extremely large. Thus the method is computationally impractical even for a one-particle basis with a moderate size. One possibility to avoid this problem is to truncate the expansion of the wave function. A systematic approach is to include all determinants up to n-times excited ones. The simplest such truncation is called singly and doubly-excited CI (SDCI). As the name suggests, the expansion is truncated at triply excited determinants. The effect of singly-excited states on the correlation energy is in general minor as they do not couple directly to the HF ground-state due to Brillouin's theorem [3]. However, they do couple indirectly to the HF ground-state via doubly-excited states. Therefore one can in principle neglect the contribution of singly-excited states to the correlation energy and reduce the method to doubly-excited CI (DCI). This simplifies the resulting equations but the number of singly-excited determinants is much smaller than the one of doubly-excited so that they may as well be kept in the expansion.
We discussed FCI as a post-Hartree-Fock method, but in principle, any one-electron basis can be used to build the N-electron configurations. It turns out that the CI expansion obtained from HF orbitals is pretty slow converging [3]. Thus the question arises if one can find a faster converging set of orbitals. This problem was first formulated by Slater and later a solution was provided by Löwdin [50] in the form of the natural orbitals. A faster converging single-particle basis is desirable not only for FCI but also for other correlated wave function methods involving virtual orbitals.

3.3 Natural orbitals

Consider the one-electron density obtained from a normalized N-electron wave function Ψ

$$n(\mathbf{x}) = N \int d\mathbf{x}_2 ... d\mathbf{x}_N \Psi(\mathbf{x}, \mathbf{x}_2, ..., \mathbf{x}_N) \Psi^*(\mathbf{x}, \mathbf{x}_2, ..., \mathbf{x}_N), \tag{3.3.1}$$

which represents the probability to find an electron at position $\mathbf{r}$ with spin σ, summarized as $\mathbf{x} = (\mathbf{r}, \sigma)$. The pre-factor N is included to ensure that the density integrates up to the number of electrons, i.e the normalization condition $\int d\mathbf{x} n(\mathbf{x}) = N$ holds. The concept of the density can be generalized to the first-order reduced density matrix or one-electron reduced density matrix (1-RDM)

$$\gamma(\mathbf{x}, \mathbf{x}') = N \int d\mathbf{x}_2 ... d\mathbf{x}_N \Psi(\mathbf{x}, \mathbf{x}_2, ..., \mathbf{x}_N) \Psi^*(\mathbf{x}', \mathbf{x}_2, ..., \mathbf{x}_N), \tag{3.3.2}$$

which, in the special case of $\mathbf{x} = \mathbf{x}'$, reduces to the above definition (3.3.1) of the one-electron density. Thus, its diagonal elements correspond to the density. Since the 1-RDM is a two-variable function it can be expanded in the basis of the HF spin orbitals $\{\phi_i\}$

$$\gamma(\mathbf{x}, \mathbf{x}') = \sum_{i,j} \phi_i(\mathbf{x}) \gamma_{ij} \phi_j^*(\mathbf{x}'), \tag{3.3.3}$$

where the coefficient matrix (γ_{ij}) is the discrete representation of the 1-RDM in the basis of the HF orbitals. It is a hermitian matrix, which follows from its definition

$$\gamma_{ij} = \int d\mathbf{x} d\mathbf{x}' \phi_i^*(\mathbf{x}) \gamma(\mathbf{x}, \mathbf{x}') \phi_j(\mathbf{x}'). \tag{3.3.4}$$

In the special case that the wave function Ψ is just the HF or KS ground-state wave function, i.e. a single Slater-determinant, the 1-RDM becomes particularly simple

$$\gamma^{HF}(\mathbf{x}, \mathbf{x}') = \sum_{i}^{occ.} \phi_i(\mathbf{x}) \phi_i^*(\mathbf{x}'). \tag{3.3.5}$$

This follows directly from the definition (3.3.2) and the fact that the HF spin-orbitals are orthonormal. Hence, the discrete representation of the Hartree-Fock 1-RDM in the HF spin-orbital basis is just a diagonal matrix, with ones for the occupied orbitals and zeros for the virtual orbitals

$$\begin{aligned} \gamma_{ij}^{HF} &= \delta_{ij} \quad \text{for } i, j \in \text{occupied} \\ \gamma_{ij}^{HF} &= 0 \quad \text{else.} \end{aligned} \tag{3.3.6}$$

Therefore, the diagonal elements are interpreted as the occupation numbers of the corresponding orbitals. For a general (CI) wave function, the discrete representation in the HF spin-orbital basis is not necessarily diagonal. However, since the matrix is hermitian it can be diagonalized. This is equivalent to defining a different basis $\{\chi_i\}$ in which the discrete representation of the 1-RDM becomes diagonal. This new basis is related to the HF basis via a unitary transformation U

$$\begin{aligned} \phi_i &= \sum_k \chi_k U^\dagger_{ki} \\ \chi_i &= \sum_k \phi_i U_{ki}. \end{aligned} \tag{3.3.7}$$

The set of orthonormal functions, in which the matrix representation of the 1-RDM is diagonal, are called the natural orbitals. By substituting the transformation (3.3.7) into (3.3.3) we find the representation of the 1-RDM with respect to the new basis

$$\begin{aligned} \gamma(\mathbf{x}, \mathbf{x}') &= \sum_{ijkl} \chi_k(\mathbf{x}) U^\dagger_{ki} \gamma_{ij} U_{jl} \chi_l(\mathbf{x}') \\ &= \sum_{kl} \chi_k(\mathbf{x}) \left(U^\dagger \gamma U \right)_{kl} \chi_l(\mathbf{x}') \\ &= \sum_{kl} \chi_k \eta_{kl} \chi_l(\mathbf{x}'). \end{aligned} \tag{3.3.8}$$

Here $\eta = U^\dagger \gamma U$ denotes the matrix representation of the 1-RDM in the new basis $\{\chi_i\}$. Since γ is Hermitian we can find a unitary transformation U such that η is diagonal

$$\eta_{ij} = \eta_i \delta_{ij}. \tag{3.3.9}$$

The basis functions that diagonalize the matrix representation of the one-particle reduced density matrix, are called the natural orbitals. Analogous to (3.3.6) we can interpret the eigenvalues of the 1-RDM η_i as the occupation number of the i-th natural orbital [50]. They can range from 0 to 1 and further fulfill $\sum_i \eta_i = N$. Thus, more than the N lowest natural orbitals are in general occupied by electrons. From now on we assume that the list of natural orbitals is ordered by decreasing occupation number, i.e $\eta_i \geq \eta_{i+1}$. The so defined set of orbitals has some optimum properties, the most important being that they yield the most rapid converging CI expansion [3, 51]. This means that constructing the configurations in the CI expansion using natural orbitals reduces the number of determinants needed to obtain an accurate representation of the interacting wave function.

Furthermore, one can show that only determinants that are constructed from natural orbitals with large occupation numbers make a significant contribution to the energy. Thus it is reasonable to truncate the set of natural orbitals at some small occupation numbers. Still, to obtain natural orbitals one needs to find the unitary matrix U that diagonalizes the $1 - RDM$. Hence one needs to construct the one-particle reduced density matrix, which in turn requires the knowledge of the wave function. Since we want to use the natural orbitals to obtain a fast converging CI expansion of the wave function the whole concept seems redundant. Luckily it turns out that approximated natural orbitals are almost as good as the exact ones. Thus, different schemes to approximate natural orbitals have been investigated in the past. One possibility to obtain approximated natural orbitals is by iteration. Starting with an initial guess for the natural orbitals one constructs an approximated CI wave function including a reasonable number of configurations. For this wave function, the natural orbitals are calculated, which serve as a basis for the next iteration. This scheme was proposed by Davison and Bender in 1966 [52]. The convergence behavior of such schemes is discussed in detail by Thunemann et al. [53]. Note that Löwdin proposed in his paper an approach to calculate natural orbitals without requiring the knowledge of the wave function [50]. He came up with a set of coupled integrodifferential equations for the natural orbitals. However, a different approach to obtain approximate natural orbitals, that involves approximating the one-particle reduced density matrix is discussed in the next section.

3.3.1 RPA natural orbitals

The idea of this approach is to express the one-particle reduced density matrix using Green's functions. As the interacting Green's function is given by a Dyson equation, this yields a native perturbation expansion of the 1-RDM in terms of the independent particle Green's function and the self-energy. The expansion is truncated at the first-order and the self-energy is approximated by the RPA self-energy. This gives an expression for the RPA reduced density matrix, which can be diagonalized to obtain RPA natural orbitals (RPA-NOs) [42].
The first important observation is that the 1-RDM is related to the interacting Green's function. Therefore we start with the definition of the Green's function

$$G(\mathbf{r}, \mathbf{r}', t - t') = -i \left\langle \Psi_0 \middle| \hat{T}\{\hat{\Psi}(\mathbf{r}, t)\hat{\Psi}^\dagger(\mathbf{r}', t') \middle| \Psi_0 \right\rangle \tag{3.3.10}$$

where Ψ_0 denotes the ground-state wave function. The $\hat{\Psi}^\dagger$, $\hat{\Psi}$ are the field operators, which are defined as a linear combination of the creation and annihilation operators $\hat{a}_k^\dagger$, $\hat{a}_k$

respectively. Note that the latter are given in the Heisenberg picture. Since they create or annihilate a particle in a single-particle state labeled by the quantum number k, we conclude that the field operators create or annihilate a particle in a superposition of all single-particle states. In other words, they create or annihilate a particle that is fully localized at position $\mathbf{r}$ at time t. Further, $\hat{T}$ denotes the time-order operator, which orders the creation and annihilation field operators such that the time difference is positive. It takes care of the causality of the actions of the two field operators.
To see the connection between the Green's function and the 1-RDM we need the write down the latter in the second quantization

$$\gamma(\mathbf{r}, \mathbf{r}') = \left\langle \Psi_0 \middle| \hat{\Psi}^\dagger(\mathbf{r}')\hat{\Psi}(\mathbf{r}) \middle| \Psi_0 \right\rangle, \tag{3.3.11}$$

where Ψ denotes the wave function. By inserting a completeness relation over all many-body states between the field operators, it can easily be shown that the above definition is indeed equivalent to Eq. (3.3.2). Comparing both the definition of the Green's function (3.3.10) and the definition of the 1-RDM in the second quantization (3.3.11) we find that

$$\gamma(\mathbf{r}, \mathbf{r}') = -i \lim_{\tau \to 0^-} G(\mathbf{r}, \mathbf{r}', \tau). \tag{3.3.12}$$

The superscript 0^- denotes that the time-difference τ approaches zero from below. This ensures that the two field-operators are interchanged by the time-order operator. Thus, in the limit of small negative time-differences, the 1-RDM is obtained from the Green's function. Recall that the interacting Green's function is determined by a Dyson equation involving the independent particle Green's function [12], denoted by G^0, and the self-energy Σ

$$G(2,1) = G^0(2,1) + G^0(2,\bar{3})\Sigma(\bar{3},\bar{4})G(\bar{4},1). \tag{3.3.13}$$

A shorthand notation is used $\{r_1, t_1\} = 1$, and the bars on top of the coordinates indicate integration over those. Plugging this Dyson equation into (3.3.12) we find a perturbation expansion of the 1-RDM in terms of the independent particle Green's function and the self-energy

$$\gamma = \gamma^0 - i \lim_{\tau \to 0^-} \left[G^0\Sigma G^0 + G^0\Sigma G^0\Sigma G^0 + ... \right]. \tag{3.3.14}$$

The zero-order term corresponds to the independent particle Green's function in the Dyson equation. Thus, γ^0 might be interpreted as the non-interacting 1-RDM corresponding to a

system of independent particles [42]. Recall that the 1-RDM becomes particularly simple if the wave function is a single Slater determinant. Therefore we express the independent one-particle reduced density matrix in terms of the occupied single-particle orbitals (e.g HF or DFT orbitals)

$$\gamma^0(\mathbf{r},\mathbf{r}') = -i \lim_{\tau\to 0^-} G^0(\mathbf{r},\mathbf{r}',\tau) = \sum_i^{occ.} \phi_i(\mathbf{r})\phi_i^*(\mathbf{r}'). \tag{3.3.15}$$

By including higher-order terms in the expansion of the 1-RDM (3.3.14), one improves on γ^0. For now, we will have a look at the first-order correction to the full 1-RDM. While the independent particle Green's function in its spectral representation is given in terms of all single-particle orbitals (both occupied and unoccupied), the self-energy still needs to be approximated. Choosing the RPA self-energy as an approximation, one finds the RPA one-particle reduced density matrix

$$\gamma^{RPA}(\mathbf{r},\mathbf{r}') = -i \lim_{t\to 0^-} \left[G^0 + G^0\Sigma^{RPA}G^0\right](\mathbf{r},\mathbf{r}',\tau). \tag{3.3.16}$$

Recall that the RPA self-energy is calculated from the independent particle Green's function and the RPA screened interaction W^{RPA}, which corresponds to W^0 in the first self-consistency cycle of a GW calculation [42]

$$\Sigma^{RPA}(1,2) = G^0(1,2)W^0(2,1). \tag{3.3.17}$$

Therefore, only the independent-particle Green's function, calculated from the single-particle orbitals of an underlying DFT calculation, is needed to evaluate the RPA 1-RDM. It is used to calculate the independent-particle polarizability χ^0 (see Eq. (2.2.9)) and further the RPA screened interaction W^0. Next, the RPA self-energy can be evaluated using Eq. (3.3.17 as well as the first-order correction to the 1-RDM in the random-phase approximation. Finally, diagonalizing the RPA 1-RDM yields the RPA-NOs, which can be used as a single-orbital basis for a follow-up high-level correlated method.

Chapter 4

RPA and RPA-NO calculations

The goal of the practical part of this thesis was to explore various approaches to obtain consistent atomization energies for a set of small molecules using the RPA implementation in VASP. Therefore, a reduced set of molecules of the Gaussian-2 test set [54] was selected. This molecular set is a popular benchmark in quantum chemistry because its atomization energies are well established. It includes in total 55 molecules, from which 30, involving first- and second-row elements, were picked. We performed the RPA calculations using both standard orbitals from an underlying DFT calculation and RPA natural orbitals. The molecular geometries were taken from the supplementary of a paper of Nemec et al. [55] and the obtained total RPA atomization energies are compared to results published by Bates et al. [1] in 2013 and Ren et al. [40] in 2012. In a private communication with Bates we received updated results regarding their 2013 paper. Those will be used as reference throughout this thesis.

4.1 RPA atomization energies for the G2 test set

There are various parameters, which affect the RPA calculations of the molecules. Since VASP relies on the projector-augmented-wave (PAW) method [56], the choice of the pseudo-potential for the core states is important. Furthermore, as VASP is designed for calculations on solids, also the cell size needs to be large enough to avoid interactions between the periodic replicas of the molecules. Finally, the energy cutoff, determining the size of the plane-wave basis set, is crucial to obtain properly converged results. To analyze the impact of these parameters on the results, we varied only one of them at a time. Starting with a proper convergence analysis of the pseudo-potentials, the impact of the plane-wave cutoff and the cell size on the RPA correlation energy differences were

examined next. Finally, we investigated extrapolation methods to obtain better-converged correlation energies. Note that the calculations are done for one k point at Γ and without dipole corrections.
Although an RPA calculation in VASP yields the Hartree-Fock plus the RPA correlation energy, we decided to converge the HF total energy separately. The reason being that the RPA calculations are way more expensive compared to standard DFT calculations. Therefore, it is impractical to converge both the HF and the RPA correlation energy in the actual RPA calculation. Better total atomization energies may be obtained by separately calculating accurate HF energies and adding those to the correlation energies obtained in the RPA calculations (see Eq. (4.1.1)). This is justified because the random-phase approximation does not rely on error cancellations between the exchange and correlation energy as the traditional LDA functionals do. The HF energy functional is evaluated with previously obtained PBE orbitals. We call this the Hartree exact exchange energy (HXX@PBE) based on the quantum chemistry terminology. Self-consistent PBE orbitals are used as a single-particle orbital basis for the RPA calculation.

$$E^{RPA} = E^{HXX} + E_c^{RPA} \tag{4.1.1}$$

Since it is hard to converge total correlation energies and because VASP uses pseudo-potentials, we focus on the atomization energies of the molecules. Those are given as the difference between the total energy of the molecule and the energies of the individual atoms. For example, the CO_2 atomization energy is calculated as

$$\Delta E^{\mathrm{CO_2}} = E^{\mathrm{CO_2}} - E^{\mathrm{C}} - 2E^{\mathrm{O}}. \tag{4.1.2}$$

Note that we converge the HXX energy separately, thus it can be treated independently. Therefore, in the RPA setp only the correlation contribution ($\Delta E_c^{\mathrm{CO_2}} = E_c^{\mathrm{CO_2}} - E_c^{\mathrm{C}} - 2E_c^{\mathrm{O}}$) to the above definition of the atomization energy is of interest. For convenience, we still call this (correlation) atomization energy or correlation energy difference.

4.1.1 Choice of the pseudo-potentials

We have evaluated three sets of potentials: two different sets of hard PAW potentials and a set of hard GW potentials as seen in Tab. (4.1). For H, Li and Be we have chosen hard and sv_GW potentials respectively. The latter potentials are recommended for alkali- and alkali-earth metals, since these treat the semi-core s and p states as valence states. We are aware that the hard PAW potentials will probably yield worse correlation energies than

Atom	1st set	2nd set	3rd set
H	H_h	H_h	H_h
Li	Li_sv_GW	Li_sv_GW	Li_sv_GW
Be	Be_sv_GW	Be_sv_GW	Be_sv_GW
C	C_h_new	C_h_new*	C_h_GW
N	N_h_new	N_h_new*	N_h_GW
O	O_h_new	O_h_new*	O_h_GW
F	F_h_new	F_h_new*	F_h_GW

Table 4.1: List of potentials used for the different sets of calculations.

the hard GW potentials since those are specifically designed for RPA and GW calculations. Nevertheless, we had hoped that the hard PAW potentials have a superior convergence behavior because they are softer than the hard GW potentials.

After some initial tests with standard hard PAW potentials, we decided to evaluate hard PAW potentials specifically designed for our purpose. We ended up generating two sets of PAW potentials with two s and p partial waves. For the first set (in the lack of a better name called h_new), the second p partial waves were placed well above the vacuum level, for instance for C 15 Ry above the vacuum level, for F 11 Ry above the vacuum level. This results in an excellent description of the scattering properties up to about 20 Ry above the vacuum level. As shown in Tab. (4.2), these potentials yield excellent agreement with reference HF calculations by Nemec et al. [55]. We report a root mean square deviation (RMS) of 13 meV for this potentials compared to Nemec. However, the downside of these potentials is that the convergence with respect to the plane wave cutoff is rather slow, as shown in Tab. (4.3): evaluating the HF energy functional using PBE orbitals shows a strong plane-wave cutoff dependence. For instance, for CO_2 the HXX energy changes by 260 meV when the energy cutoff is increased from 600 eV to 800 eV. This slow convergence would make the RPA calculations rather expensive. Therefore, we decided to also evaluate a set of potentials (called h_new*), where the second p partial wave is placed roughly at the binding energy of the 2s orbitals (the first one is placed at the eigenenergy of the 2p eigenstates). A reasonable compromise was found by placing the p partial wave at -1.5 Ry for N, O, and F, and -1.2 Ry for C.

As indicated in Table (4.2), this somewhat deteriorates the results for the self-consistent HF calculations resulting in a RMS deviation of 28 meV compared to Nemec. The binding energies are now up to 60 meV below the results of Nemec [55]. We attribute this to the reduced flexibility of the p-orbitals for the second set of potentials. However, this reduced flexibility goes in hand with a much-improved plane wave convergence as seen in Table (4.3). Now the errors for the HXX energies are reduced to 90 meV between 600 eV and

Molecules	**h_new**	**h_new***	**h_GW**	**Nemec**
BeH	-2.1899	-2.1899	-2.1905	-2.1893
C2H2	-12.7246	-12.6634	-12.6807	-12.7182
C2H4	-18.5338	-18.4710	-18.4947	-18.5246
C2H6	-23.8852	-23.8205	-23.8505	-23.8493
CH2_singlet	-5.4920	-5.4762	-5.4793	-5.4977
CH2_triplet	-6.7103	-6.6919	-6.6991	-6.7210
CH3	-10.5232	-10.4974	-10.5088	-10.5323
CH4	-14.2185	-14.1857	-14.2029	-14.2190
CN	-3.9141	-3.8758	-3.8843	-3.8958
CO2	-10.6669	-10.6066	-10.6355	-10.6559
CO	-7.5107	-7.4745	-7.4926	-7.4973
F2	1.6049	1.6125	1.6207	1.6161
H2CO	-11.1466	-11.1050	-11.1205	-11.1423
H2O2	-5.7985	-5.7825	-5.7827	-5.8036
H2O	-6.7388	-6.7287	-6.7303	-6.7525
H3COH	-15.9965	-15.9557	-15.9681	-15.9973
HCN	-8.6313	-8.5818	-8.5974	-8.6201
HCO	-7.8798	-7.8422	-7.8544	-7.8702
HF	-4.1891	-4.1818	-4.1845	-4.1984
Li2	-0.1664	-0.1664	-0.1664	-0.1642
LiF	-3.9143	-3.9093	-3.8997	-3.9292
LiH	-1.4793	-1.4793	-1.4797	-1.4847
N2	-5.0044	-4.9671	-4.9779	-4.9737
N2H4	-11.6030	-11.5697	-11.5818	-11.5927
NH2	-5.0909	-5.0790	-5.0866	-5.0999
NH3	-8.7001	-8.6826	-8.6921	-8.7080
NH	-2.2163	-2.2101	-2.2146	-2.2228
NO	-2.3061	-2.2837	-2.2909	-2.2883
O2	-1.4190	-1.4059	-1.4108	-1.4067
OH	-2.9527	-2.9474	-2.9522	-2.9649
RMS	0.0130	0.0277	0.0178	/

Table 4.2: Self-consistent HF atomization energies for a subset of G2 molecules calculated with VASP. The calculations have been performed using different pseudo-potentials, in a 15 Å cell and at a 800 eV cutoff. The results are given in eV and are compared to self-consistent HF results published by Nemec et al. [55]. They report a basis set error below 0.1 kcal/mol for first row atoms using the ADF/QZ4P basis set. The root-mean-square error (RMS) of each column compared to Nemec is given in the final row.

	h_new		**h_new***		**h_GW**		**Bates**
Molecules	600 eV	800 eV	600 eV	800 eV	600 eV	800 eV	cc-pV5Z
BeH	-2.1422	-2.1351	-2.1422	-2.1351	-2.1422	-2.1351	-2.1348
C2H2	-12.4913	-12.6124	-12.4967	-12.5618	-12.5142	-12.5970	-12.6001
C2H4	-18.2506	-18.3989	-18.2585	-18.3465	-18.2785	-18.3842	-18.4247
C2H6	-23.6231	-23.7783	-23.6284	-23.7241	-23.6544	-23.7636	-23.7815
CH2_singlet	-5.4126	-5.4536	-5.4136	-5.4407	-5.4167	-5.4462	-5.4371
CH2_triplet	-6.6318	-6.6823	-6.6333	-6.6674	-6.6414	-6.6813	-6.6885
CH3	-10.4374	-10.5067	-10.4399	-10.4852	-10.4496	-10.5019	-10.5109
CH4	-14.0981	-14.1883	-14.1017	-14.1604	-14.1140	-14.1809	-14.1900
CN	-3.0028	-3.0907	-3.0447	-3.0603	-3.0209	-3.0589	-3.0687
CO2	-9.8667	-10.1283	-10.0703	-10.0803	-9.9714	-10.1085	-10.0726
CO	-7.1839	-7.3005	-7.2794	-7.2703	-7.2405	-7.2867	-7.3083
F2	1.9104	1.8535	1.8315	1.8582	1.7903	1.8486	1.8282
H2CO	-10.7180	-10.8963	-10.8166	-10.8628	-10.7673	-10.8802	-10.8875
H2O2	-5.4237	-5.5736	-5.5711	-5.5637	-5.4997	-5.5576	-5.5568
H2O	-6.5977	-6.7051	-6.6932	-6.6982	-6.6393	-6.6941	-6.6959
H3COH	-15.6305	-15.8240	-15.7296	-15.7915	-15.6825	-15.8048	-15.8150
HCN	-8.3356	-8.4556	-8.3773	-8.4151	-8.3687	-8.4300	-8.4278
HCO	-7.4430	-7.5893	-7.5381	-7.5589	-7.4919	-7.5734	-7.5860
HF	-4.0827	-4.1591	-4.1749	-4.1542	-4.1241	-4.1595	-4.1474
Li2	-0.1456	-0.1458	-0.1455	-0.1458	-0.1456	-0.1458	-0.1459
LiF	-3.6935	-3.7595	-3.7772	-3.7576	-3.7251	-3.7527	-3.7704
LiH	-1.4721	-1.4616	-1.4597	-1.4616	-1.4721	-1.4616	-1.4615
N2	-4.7099	-4.8208	-4.7935	-4.7912	-4.7565	-4.7828	-4.7563
N2H4	-11.2399	-11.4386	-11.3409	-11.4135	-11.2872	-11.3988	-11.4190
NH2	-4.9683	-5.0346	-5.0033	-5.0255	-4.9858	-5.0204	-5.0230
NH3	-8.5577	-8.6622	-8.6113	-8.6487	-8.5852	-8.6423	-8.6516
NH	-2.1284	-2.1602	-2.1457	-2.1556	-2.1364	-2.1525	-2.1531
NO	-1.8766	-2.0003	-1.9950	-1.9838	-1.9328	-1.9759	-1.9663
O2	-0.9428	-1.0836	-1.0790	-1.0763	-1.0442	-1.0791	-1.0605
OH	-2.8645	-2.9157	-2.9132	-2.9121	-2.8870	-2.9119	-2.9097
RMS	0.1086	0.0213	0.0602	0.0255	0.0718	0.0152	/

Table 4.3: HXX atomization energies for a subset of G2 molecules calculated with VASP. They are compared for two different plane-wave cutoffs and between three sets of pseudo-potentials. The calculations have been performed in a 15 Å cell. The results are given in eV and are compared to HXX results published by Bates et al. [1] using a cc-pV5Z Gaussian basis set. The root-mean-square error (RMS) of each column and the results of Bates et al. are given in the final row.

800 eV, which is acceptable. Furthermore, the HXX results show acceptable agreement with the reference values of Bates et al. [1]. The largest deviations are reported for C_2H_4 and C_2H_6 (79 meV and 57 meV too low compared to Bates et al.), while the remaining atomization energies agree within 40 meV. Note that the reference values were calculated with highly accurate correlation-consistent quintuple-zeta basis functions (cc-pVQZ) [57]. For now, the focus was to investigate the convergence behavior of the potentials, such that the RPA calculations later show good convergence. Note that the actual HXX energies, which are then added to the final RPA correlation energies, were evaluated at a higher cutoff and in a larger cell.

The final evaluated set has been the hard GW potentials, which are specifically designed for RPA and GW calculations. Hence, we expect them to yield better RPA correlation energies and hopefully as good HXX energies as the previously tested PAW potentials. The obtained self-consistent HF atomization energies shown in Tab. (4.2) are up to 40 meV below those of Nemec. Their convergence at the HXX@PBE level with respect to the plane-wave basis size is found in Tab. (4.3). They seem to be a compromise between the two previously evaluated sets of potentials. For CO_2 we again report a sizable error of 110 meV between a 600 eV and 800 eV energy-cutoff. This indicates mediocre convergence behavior, as already expected. The HXX results are in good agreement with the ones obtained by Bates et al. The deviation of our results using the h_GW potentials compared to Bates et al. is below 43 meV, i.e. within chemical precision. Here the atomization energy of C_2H_4 shows the largest discrepancy, being 41 meV too low.

We conclude that the h_new PAW potentials, although they yield self-consistent HF energies in excellent agreement with Nemec, show a too slow convergence behavior with respect to the plane-wave cutoff at the HXX@PBE level. This indicates that probably large energy cutoffs are required for decently converged RPA correlation energies, which is not feasible. The second set of PAW potentials is less flexible in the p orbitals and thus does not reproduce the self-consistent HF energies as precisely as the previous potentials. However, this results in a faster convergence of the HXX energies: ~90 meV difference in contrast to up to 260 meV. The hard GW potentials seem to be a compromise between the previous potentials. Their self-consistent HF energies are also too low but not as severe as those of the second PAW potentials: we report a root mean square deviation of 28 meV compared to 21 meV. However, the HXX energies converge slower than those of the h_new* potentials. Nevertheless, the hard GW potentials seem to reproduce the HXX atomization energies obtained by Bates et al. better: at 800 eV cutoff we report a root mean square deviation compared to Bates et al. of 26 meV and 15 meV respectively. While for the h_GW potentials all molecular atomization energies are within chemical precision

to the results of Bates et al., we report deviation larger than 1 kcal/mol for both C_2H_4 and C_2H_6 using the h_new* potentials. Thus, we decided to evaluate both the newly generated h_new* and the h_GW potentials in the RPA calculations. We are aware that the GW potentials will probably yield overall better RPA correlation energies. However, since they converge slower at the Hartree-Fock level, the hard PAW potentials might be a good trade-off between decent correlation energies and computational efficiency.

4.1.2 Plane-wave cutoff and cell size

The molecules were placed at the center of a cubic cell with broken symmetry. To avoid interactions of neighboring replicas of the molecules, a large enough box has to be chosen. Although the cell size does not significantly affect the computational cost at the DFT level it certainly does in the RPA calculations. Therefore we had to restrict our calculations to 8 Å and 9 Å boxes. Note that this refers to the lattice constant and not the actual volume of the box. In principle, larger cell sizes could be achieved by lowering the plane-wave cutoff. However, this would not improve the accuracy of the correlation energies as those show a strong energy cutoff dependence. Thus, a good balance between the cell size and the plane-wave cutoff needs to be maintained. It turned out that we could afford RPA calculations in an 8 Å box with a cutoff up to 800 eV. Restricting the cutoff to 700 eV we could increase the cell to 9 Å. The corresponding HXX energies were calculated in a 15 Å cell with a 800 eV plane-wave cutoff. The PAW and GW potentials were compared in a 8 Å box both at a 600 eV and 700 eV cutoff. We judged both their convergence behavior and their agreement with the reference values of Bates et al. [1]. The results are found in Table 4.4. For both sets of potentials, the correlation energy differences converge up to 50 meV between the two evaluated cutoffs, which is acceptable. CO_2, F_2 and NO seem to be rather slow converging while Li_2 and LiH are pretty much converged at 600 eV. However, compared to the reference values of Bates et al., we find that the hard GW potentials show significant better agreement: at a 700 eV cutoff we report a root mean square deviation compared to Bates et al. of 83 meV and 52 meV respectively. Unfortunately, both sets of potentials do not reproduce the reference values within chemical accuracy (1 kcal/mol $\approx$ 43 meV). The hard GW potentials yield atomization energies for most molecules within 80 meV with those of Bates et al. The molecules N_2H_4 and H_2O_2 show larger deviations over 100 meV.

Keeping the plane-wave cutoff at 700 eV, we also evaluated the atomization energies using a 9 Å box. The results are compared to the 8 Å values in Table (4.5). We find that the hard GW potentials seem to be already converged up to a few meV for the 8 Å box, while

	h_new*		**h_GW**		**Bates**
Molecules	600 eV	700 eV	600 eV	700 eV	cc-pV5Z
BeH	-2.2653	-2.2667	-2.2653	-2.2667	-2.1728
C2H2	-16.4583	-16.4599	-16.5260	-16.5340	-16.5293
C2H4	-23.1962	-23.1927	-23.2623	-23.2652	-23.3142
C2H6	-29.5527	-29.5479	-29.6208	-29.6221	-29.6741
CH2_singlet	-7.5646	-7.5601	-7.5732	-7.5731	-7.5890
CH2_triplet	-7.7644	-7.7605	-7.7888	-7.7872	-7.8012
CH3	-12.7325	-12.7287	-12.7629	-12.7618	-12.7840
CH4	-17.5080	-17.5041	-17.5438	-17.5429	-17.5707
CN	-7.4012	-7.4175	-7.4159	-7.4372	-7.4658
CO2	-15.5953	-15.6512	-15.6999	-15.7503	-15.7989
CO	-10.5024	-10.5322	-10.5522	-10.5803	-10.5947
F2	-1.2474	-1.2719	-1.2104	-1.2583	-1.3093
H2CO	-15.3050	-15.3260	-15.3648	-15.3849	-15.4239
H2O2	-10.9444	-10.9769	-10.9844	-11.0143	-11.1188
H2O	-9.5863	-9.6041	-9.6203	-9.6347	-9.7050
H3COH	-21.1487	-21.1627	-21.2108	-21.2255	-21.3054
HCN	-12.8906	-12.9065	-12.9292	-12.9487	-12.9522
HCO	-11.2794	-11.3019	-11.3344	-11.3575	-11.4299
HF	-5.6679	-5.6839	-5.6836	-5.7059	-5.7653
Li2	-0.7648	-0.7650	-0.7648	-0.7648	-0.8266
LiF	-5.5665	-5.5813	-5.5721	-5.5918	-5.6052
LiH	-2.4528	-2.4528	-2.4528	-2.4527	-2.4485
N2	-9.6221	-9.6580	-9.6215	-9.6599	-9.6705
N2H4	-18.3799	-18.3974	-18.4006	-18.4186	-18.5248
NH2	-7.7397	-7.7429	-7.7446	-7.7477	-7.7827
NH3	-12.5399	-12.5481	-12.5532	-12.5615	-12.6237
NH	-3.5598	-3.5607	-3.5608	-3.5614	-3.5769
NO	-6.3295	-6.3603	-6.3449	-6.3755	-6.4087
O2	-4.8029	-4.8352	-4.8203	-4.8467	-4.9058
OH	-4.4425	-4.4504	-4.4655	-4.4725	-4.4964
RMS	0.0976	0.0831	0.0672	0.0517	/

Table 4.4: RPA atomization energies in eV for a subset of G2 molecules calculated with VASP. The correlation energies have been obtained for a 8 Å box with both a 600 eV and 700 eV plane-wave cutoff. The RPA correlation energies have been added to the previously obtained HXX energies (800 eV, 15 Å), see Tab. (4.3). The reference values are reported by Bates et al. [1]. The root-mean-square error (RMS) of each column compared to Bates et al. is given in the final row.

the hard PAW potentials still change up to 20 meV. Larger changes for both sets are reported for the molecules BeH, Li_2, LiF, LiH. The atomization energies of these molecules changed up to 40 meV by increasing the cell size. The reason for this is probably the "size" of these molecules. Both Li and Be have fairly large atomic orbitals, with tails that are still sizable beyond half the box size. Thus the cell size might still be too small.
As expected, the hard PAW potentials yield worse correlation energies than the hard GW potentials when compared to the reference values of Bates et al. Unfortunately, this comes without a trade-off in form of a faster convergence. Thus we decided to only further evaluate the hard GW potentials as they seem to be converged for 8 Å cells. This leaves room to further improve the atomization energies by increasing the plane-wave basis set.

4.1.3 Extrapolated correlation energies

Now that we have settled for the set of hard GW potentials, we investigated strategies to improve on the correlation atomization energies. Bates et al. had obtained their correlation energies by extrapolating between the cc-pVQZ and cc-pV5Z Gaussian basis sets [38]. Thus we decided to investigate similar schemes to obtain extrapolated correlation energies. There are three different cutoffs at play in VASP when doing an RPA calculation. First of all, there is the general energy cutoff E_{cut}, which controls the size of the plane-wave basis. The second cutoff is governed by the flag ENCUTGW or E^{χ}_{cut}. It sets the maximum energy of a reciprocal lattice vector ($\mathbf{G}$ vector) to be included in the calculation of the independent particle response function χ^0. By default, it is set to $\frac{2}{3}$ of the plane-wave cutoff. Since the RPA correlation energy strongly depends on E^{χ}_{cut}, VASP has a built-in extrapolation with respect to this cutoff. It internally varies E^{χ}_{cut} between its maximum and some smaller values and evaluates the corresponding correlation energies. Those are then extrapolated to an infinite $\mathbf{G}$ vector cutoff E_c^{∞} according to [58]

$$E_c^{RPA}(E^{\chi}_{cut}) = E_c^{\infty} + \frac{A}{(E^{\chi}_{cut})^{3/2}}. \tag{4.1.3}$$

Here E_c^{∞} and A are constants to be determined. The former represents the correlation energy at an infinite cutoff of the response function. Note that there is also a third cutoff, ENCUTGWSOFT, which controls a smooth truncation of the Coulomb kernel. Since increasing the cutoff suddenly introduces a bunch of new reciprocal lattice vectors, the energy may improve abruptly leading to rough E_c^{RPA} versus cutoff curves. This is bypassed by slowly truncating the Coulomb kernel between ENCUTGWSOFT and ENCUTGW. Note that the internal extrapolation described by Eq. (4.1.3) only works reliably for the default settings of ENCUTGW and ENCUTGWSOFT. This becomes obvious in Fig. (4.1),

	h_new*		**h_GW**		**Bates**
Molecules	8 Å	9 Å	8 Å	9 Å	cc-pV5Z
BeH	-2.2667	-2.2446	-2.2667	-2.2446	-2.1728
C2H2	-16.4599	-16.4683	-16.5340	-16.5339	-16.5293
C2H4	-23.1927	-23.2039	-23.2652	-23.2678	-23.3142
C2H6	-29.5479	-29.5623	-29.6221	-29.6277	-29.6741
CH2_singlet	-7.5601	-7.5686	-7.5731	-7.5772	-7.5890
CH2_triplet	-7.7605	-7.7646	-7.7872	-7.7869	-7.8012
CH3	-12.7287	-12.7340	-12.7618	-12.7628	-12.7840
CH4	-17.5041	-17.5112	-17.5429	-17.5457	-17.5707
CN	-7.4175	-7.4322	-7.4372	-7.4474	-7.4658
CO2	-15.6512	-15.6702	-15.7503	-15.7572	-15.7989
CO	-10.5322	-10.5419	-10.5803	-10.5823	-10.5947
F2	-1.2719	-1.2782	-1.2583	-1.2646	-1.3093
H2CO	-15.3260	-15.3392	-15.3849	-15.3905	-15.4239
H2O2	-10.9769	-10.9957	-11.0143	-11.0264	-11.1188
H2O	-9.6041	-9.6122	-9.6347	-9.6389	-9.7050
H3COH	-21.1627	-21.1787	-21.2255	-21.2327	-21.3054
HCN	-12.9065	-12.9155	-12.9487	-12.9534	-12.9522
HCO	-11.3019	-11.3190	-11.3575	-11.3657	-11.4299
HF	-5.6839	-5.6857	-5.7059	-5.7076	-5.7653
Li2	-0.7650	-0.7752	-0.7648	-0.7752	-0.8266
LiF	-5.5813	-5.5433	-5.5918	-5.5539	-5.6052
LiH	-2.4528	-2.4169	-2.4527	-2.4169	-2.4485
N2	-9.6580	-9.6631	-9.6599	-9.6652	-9.6705
N2H4	-18.3974	-18.4098	-18.4186	-18.4309	-18.5248
NH2	-7.7429	-7.7473	-7.7477	-7.7521	-7.7827
NH3	-12.5481	-12.5545	-12.5615	-12.5679	-12.6237
NH	-3.5607	-3.5630	-3.5614	-3.5637	-3.5769
NO	-6.3603	-6.3693	-6.3755	-6.3811	-6.4087
O2	-4.8352	-4.8492	-4.8467	-4.8526	-4.9058
OH	-4.4504	-4.4560	-4.4725	-4.4741	-4.4964
RMS	0.0831	0.0737	0.0517	0.0467	/

Table 4.5: RPA atomization energies in eV for a subset of G2 molecules calculated in VASP. The calculations have been performed for a 700 eV plane-wave cutoff in both a 8 Å and 9 Å cubic cell. The RPA correlation energies have been added to the previously obtained HXX energies (800 eV, 15 Å), see Tab. (4.3). The results are compared to reference values obtained by Bates et al. [1]. The root-mean-square error (RMS) of each column compared to Bates et al. is given in the final row.

where we manually tested the internal extrapolation scheme for different combinations of the two **G** vector cutoffs. Each of the three colored data-sets is obtained from a separate calculation, where the individual data-points correspond to the correlation energies at different ENCUTGW cutoffs. Those are calculated internally by VASP to perform the correlation energy extrapolation. All calculation have been performed using ENCUT = 700 eV. The black data-set is obtained for the default settings (ENCUTGW = $\frac{2}{3}$ * ENCUTGW and ENCUTGWSOFT = 0.8 * ENCUTGW). For the red and blue data-set the cutoffs have been set to (ENCUTGW = ENCUT and ENCUTGWSOFT = 0.8 * ENCUTGW) and (ENCUTGW = ENCUTGWSOFT = ENCUT) respectively. The three data sets are manually extrapolated using Eq. (4.1.3). Note that this is equivalent to the internal extrapolation done by VASP. We see that the black data points show a ENCUTGW$^{-3/2}$ dependence and are correctly extrapolated to the infinite **G** vector cutoff (at $x = 0$) using Eq. (4.1.3). Using different combinations for the cutoff settings (blue and red data-sets) the data points do not have the linear behavior, leading to incorrectly extrapolated correlation energies. This results in too small atomization energies, which differ even more from those of Bates et al. Therefore we decided to keep the two **G** vector cutoffs at their default settings and to try a different extrapolation scheme. By increasing the plane-wave cutoff one indirectly increases the (default) **G** vector cutoffs. So instead of extrapolating the correlation energies at a fixed E_{cut} to infinite E_{cut}^{χ}, we tried to extrapolate to infinite E_{cut}. Therefore we calculated the (non-extrapolated) RPA correlation energies for a small set of molecules (C_2H_4, CO_2 and N_2) for cutoffs between 600 eV and 1000 eV. The obtained energies have been extrapolated with respect to E_{cut} similar to Eq. (4.1.3).

The results for the CO_2 correlation energy difference are shown in Fig. (4.2). The black data points correspond to the non-extrapolated extrapolated correlation energies calculated at five different cutoffs E_{cut}. Those are then extrapolated to infinite E_{cut} using a similar equation as Eq. (4.1.3). It is obvious that the extrapolation only works reliably for the last three data points (3-extrapolated, red line) because those show a linear behavior with respect to $E_{cut}^{-3/2}$. Including all five data points in the extrapolation (5-extrapolated, blue line) yields a too low correlation energy, which is attributed to the non-linear behavior of the first two correlation energies. The green data points correspond to the internally with respect to E_{cut}^{χ} extrapolated correlation energies at the five plane-wave cutoffs. The green dotted line represents the value to which these correlation energies converge. We can see that the 3-extrapolated and the internally extrapolated correlation energies converge to the same value within 20 meV. Using a 2-extrapolation, this difference can even be reduced to 10 meV. Thus we conclude that both extrapolation schemes are of the same

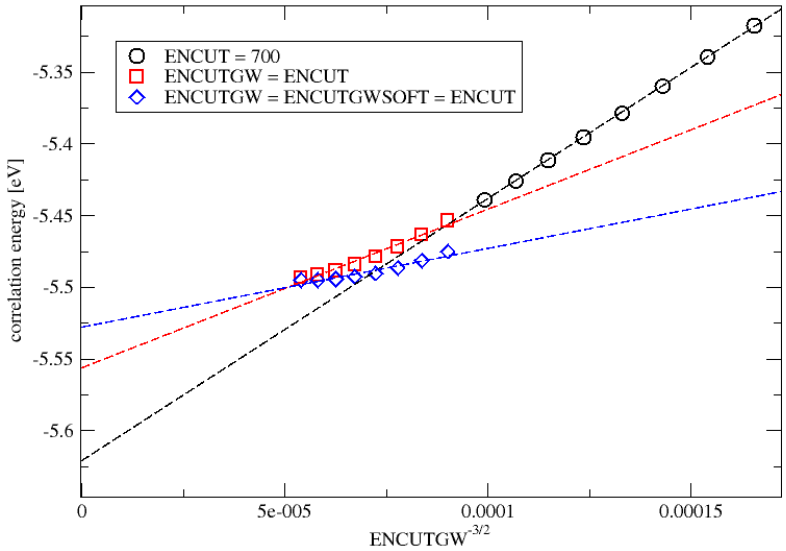

Figure 4.1: VASPs internal extrapolation scheme for RPA correlation energies tested for different settings of ENCUTGW and ENCUTGWSOFT. The extrapolated atomization energies are given at $x = 0$. The calculations are done for CO_2 with a 700 eV plane-wave cutoff and in an 8 Å cell.

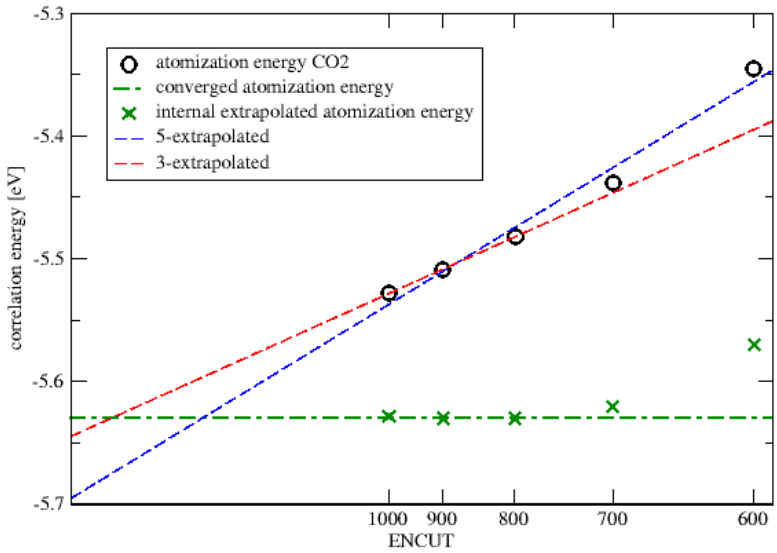

Figure 4.2: Extrapolation of the CO_2 RPA atomization energy with respect to the plane-wave cutoff. The cutoff is varied in 100 eV steps between 600 eV and 1000 eV (ENCUT$^{-3/2}$ scale). The results are compared to the internally extrapolated correlation energies.

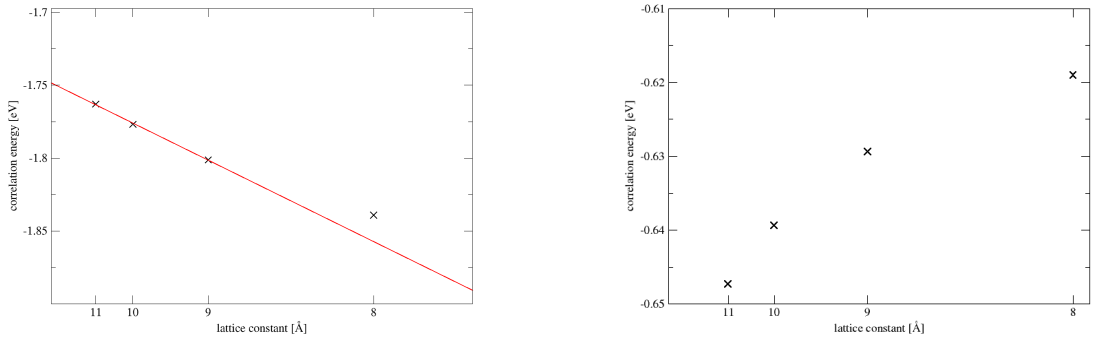

(a) (b)

Figure 4.3: Dependence of the RPA correlation energy difference on the cell size (V^{-2} scale): (a) V^{-2} behavior of LiF (b) the non-linear behavior of Li2.

quality. However, the internal extrapolation already yields converged correlation energies within 10 meV at a 700 eV plane-wave cutoff, while at least 1000 eV are required for the other scheme to work reliably. Such large cutoffs are computationally really expensive. Thus, the internal extrapolation scheme is more attractive.

As discussed in the last section, the atomization energies of most molecules are converged using a 8 Å box. Exceptions are the molecules BeH, Li_2, LiF and LiH, probably due to their spatially diffuse highest molecular orbital (Li $2s$). This causes long-range interactions between periodic replicas of the molecules even for large cells. We investigated their behavior with respect to the cell size and found that BeH, LiF and LiH show a V^{-2} volume dependence. With increasing cell size the correlation energy decreases in absolute value, which is related to the long-range van der Waals (vdW) interactions between the repeated copies of the molecules. This leads to a larger correlation energy compared to the isolated molecules. For Li_2 we could not find a similar behavior. Instead, we observed a further increase of the absolute correlation energy with respect to the cell size. This could be related to a more sizeable dispersion interaction between the atoms than between the Li_2 molecules. The behavior of the LiF and Li_2 correlation energy differences with respect to the cell size (V^{-2} scale) are shown in Fig. (4.3). The correlation energies have been evaluated for cell lattice constants between 8 Å and 11 Å. The LiF correlation energy has been extrapolated using the data points showing a V^{-2} dependence. For the 8 Å cell the interactions are probably not completely vdW-like. With larger cells the short-range interactions get insignificant and the interactions show the expected V^{-2} vdW-like behavior.

Unfortunately, this cell size extrapolation of BeH, LiH and LiF does not improve on the

Molecules	**VASP**	**VASP$_{\mathbf{ext.}}$**	**Bates**	**$\Delta_{\text{V-B}}$**	**$\Delta_{\text{V}_{\text{ext.}}\text{-B}}$**
BeH	-2.2667	-2.2224	-2.1728	-0.0939	-0.0496
LiF	-5.6006	-5.4739	-5.6052	0.0046	0.1313
LiH	-2.4572	-2.3456	-2.4485	-0.0087	0.1029

Table 4.6: Comparison of the RPA atomization energies in eV of BeH, LiF and LiH using both the 3-extrapolated and non-extrapolated correlation energies. These are added to the HXX atomization energies (20 Å and 1000 eV cutoff) found in Table (4.8). The columns $\Delta_{\text{V-B}}$ and $\Delta_{\text{V}_{\text{ext.}}\text{-B}}$ denote the errors compared to Bates et al. [1].

RPA atomization energies compared to the results of Bates et al. The 3-extrapolated atomization energies are in Table (4.6) compared to the non-extrapolated energies and to the ones published by Bates et al. While the error of the BeH atomization energy is reduced by 1 kcal/mol from 94 meV to 50 meV, are the extrapolated atomization energies of LiF and LiH by more than 100 meV smaller than the ones of Bates et al. Since for most of the molecules the 8 Å cells yield converged correlation energies and the extrapolation of BeH, Li_2 LiF and LiH did not provide clear evidence that such extrapolations work properly, we decided to avoid these extrapolations to infinite cell size.
Our final RPA atomization energies for the subset of G2 molecules using the hard GW potential set can be found in Table (4.9). The RPA calculations are performed with a 800 eV cutoff in an 8 Å cell. Furthermore, the internal extrapolation scheme of VASP is used to obtain extrapolated correlation energies. The RPA correlation energies are added to HXX energies calculated in a 20 Å box with a 1000 eV plane-wave cutoff. Those are given in Table (4.8). Finally, also the PBE atomization energies, calculated in a 20 Å box with a 1000 eV plane-wave cutoff, are compared to Bates et al and Paier et al. [59].
Our PBE atomization energies in Table (4.7) show great agreement with those published by Paier et al. [59] using VASP as a root-mean-square deviation of 8 meV was found. The largest discrepancy is found for the C_2H_4 atomization energy, with it being 22 meV smaller than the reference values of Paier et al. This is probably due to different geometries since Paier et al. fully optimized their geometries [59]. Comparing VASP with both GAUSSIAN 03 (Paier G03) and TURBOMOLE (Bates) we found similar root-mean-square deviations of approximately 26 meV. This suggests that this is the inherent difference between implementations using plane-waves and Gaussian basis functions. The HXX results shown in Table (4.8) are within chemical precision (1 kcal/mol) to those of Bates et al. Once more the largest discrepancy is reported for C_2H_4. A root-mean-square deviation of 17 meV is observed, which is even smaller than the corresponding one for the PBE results (25 meV). This is somewhat expected as it is generally difficult to evaluate density-functionals using quantum chemistry codes since those are mainly designed and optimized for HF calculations.

Molecules	**VASP**	**Paier (VASP)**	**Paier (G03)**	**Bates**
BeH	-2.3979	-2.4067	-2.4110	-2.4126
C2H2	-17.9790	-17.9744	-18.0004	-17.9992
C2H4	-24.7385	-24.7609	-24.7999	-24.7985
C2H6	-31.0564	-31.0487	-31.0964	-31.0973
CH2_singlet	-7.7505	-7.7535	-7.7665	-7.7597
CH2_triplet	-8.4259	-8.4300	-8.4387	-8.4373
CH3	-13.4302	-13.4299	-13.4472	-13.4473
CH4	-18.1987	-18.1956	-18.2216	-18.2208
CN	-8.5610	-8.5644	-8.5731	-8.5740
CO2	-18.0154	-18.0135	-18.0612	-18.0678
CO	-11.6583	-11.6476	-11.6693	-11.6719
F2	-2.2967	-2.2810	-2.2983	-2.2946
H2CO	-16.7162	-16.7169	-16.7516	-16.7487
H2O2	-12.2163	-12.2113	-12.2547	-12.2455
H2O	-10.1405	-10.1342	-10.1689	-10.1530
H3COH	-22.5214	-22.5190	-22.5667	-22.5599
HCN	-14.1399	-14.1497	-14.1584	-14.1605
HCO	-12.7764	-12.7881	-12.8141	-12.8114
HF	-6.1464	-6.1360	-6.1664	-6.1535
Li2	-0.8626	-0.8629	-0.8716	-0.8693
LiF	-6.0027	-6.0016	-6.0276	-6.0257
LiH	-2.3166	-2.3200	-2.3200	-2.3204
N2	-10.5572	-10.5678	-10.5765	-10.5676
N2H4	-19.6232	-19.6309	-19.6743	-19.6637
NH2	-8.1721	-8.1828	-8.1915	-8.1809
NH3	-13.0809	-13.0830	-13.1090	-13.0993
NH	-3.8327	-3.8421	-3.8421	-3.8371
NO	-7.4548	-7.4586	-7.4803	-7.4736
O2	-6.2190	-6.2141	-6.2444	-6.2396
OH	-4.75727	-4.7570	-4.7744	-4.7633
RMS	/	0.0080	0.0282	0.0251

Table 4.7: PBE atomization energies in eV for a subset of G2 molecules calculated with VASP. The values are obtained for 20 Å cells and 1000 eV cutoff. The reported results are compared to values of Bates et al. [1] and Paier et al. [59].

Molecules	**VASP**	**Bates**	$\mathbf{\Delta}_{\text{B-R}}$
BeH	-2.1355	-2.1348	-0.0007
C2H2	-12.5901	-12.6001	0.0101
C2H4	-18.3813	-18.4247	0.0434
C2H6	-23.7646	-23.7815	0.0169
CH2_singlet	-5.4487	-5.4371	-0.0116
CH2_triplet	-6.6802	-6.6885	0.0083
CH3	-10.5026	-10.5109	0.0084
CH4	-14.1831	-14.1900	0.0069
CN	-3.0574	-3.0687	0.0113
CO2	-10.1144	-10.0726	-0.0418
CO	-7.2909	-7.3083	0.0174
F2	1.8593	1.8282	0.0311
H2CO	-10.8843	-10.8875	0.0032
H2O2	-5.5646	-5.5568	-0.0078
H2O	-6.7005	-6.6959	-0.0046
H3COH	-15.8103	-15.8150	0.0046
HCN	-8.4297	-8.4278	-0.0019
HCO	-7.5757	-7.5860	0.0103
HF	-4.1621	-4.1474	-0.0147
Li2	-0.1460	-0.1459	-0.0001
LiF	-3.7579	-3.7704	0.0125
LiH	-1.4661	-1.4615	-0.0046
N2	-4.7904	-4.7563	-0.0340
N2H4	-11.4133	-11.4190	0.0057
NH2	-5.0270	-5.0230	-0.0040
NH3	-8.6519	-8.6516	-0.0003
NH	-2.1557	-2.1531	-0.0026
NO	-1.9839	-1.9663	-0.0176
O2	-1.0829	-1.0605	-0.0224
OH	-2.9152	-2.9097	-0.0055
RMS	/	/	0.0167

Table 4.8: HXX@PBE atomization energies in eV for a subset of G2 molecules calculated with VASP. The values are obtained for 20 Å cells and 1000 eV cutoff. The reported results are compared to values of Bates et al. [1]. The column $\Delta_{\text{B-R}}$ denotes the error Δ(VASP-Bates) and the root-mean-square deviation (RMS) is given in the final row.

Molecules	**VASP**	**Bates**	**Ren**	$\Delta_{\text{V-B}}$	$\Delta_{\text{V-R}}$	$\Delta_{\text{B-R}}$
BeH	-2.2667	-2.1728	-2.1639	-0.0939	-0.1028	-0.0089
C2H2	-16.5265	-16.5293	-16.3613	0.0029	-0.1652	-0.1680
C2H4	-23.2601	-23.3142	-23.1174	0.0541	-0.1426	-0.1968
C2H6	-29.6207	-29.6741	-29.4312	0.0534	-0.1894	-0.2429
CH2_singlet	-7.5739	-7.5890	-7.5150	0.0151	-0.0589	-0.0740
CH2_triplet	-7.7846	-7.8012	-7.7275	0.0166	-0.0571	-0.0737
CH3	-12.7607	-12.7840	-12.6797	0.0233	-0.0810	-0.1043
CH4	-17.5432	-17.5707	-17.4497	0.0275	-0.0935	-0.1210
CN	-7.4361	-7.4658	-7.3762	0.0297	-0.0598	-0.0896
CO2	-15.7442	-15.7989	-15.5634	0.0547	-0.1809	-0.2355
CO	-10.5787	-10.5947	-10.4898	0.0160	-0.0889	-0.1049
F2	-1.2740	-1.3093	-1.2315	0.0353	-0.0425	-0.0778
H2CO	-15.3809	-15.4239	-15.2468	0.0430	-0.1341	-0.1771
H2O2	-11.0095	-11.1188	-10.9364	0.1093	-0.0731	-0.1824
H2O	-9.6323	-9.7050	-9.5748	0.0727	-0.0575	-0.1302
H3COH	-21.2224	-21.3054	-21.0836	0.0830	-0.1388	-0.2218
HCN	-12.9491	-12.9522	-12.8184	0.0031	-0.1306	-0.1338
HCO	-11.3532	-11.4299	-11.2877	0.0767	-0.0655	-0.1422
HF	-5.7143	-5.7653	-5.6503	0.0510	-0.0640	-0.1150
Li2	-0.7654	-0.8266	-0.7936	0.0612	0.0281	-0.0330
LiF	-5.6006	-5.6052	-5.4379	0.0046	-0.1627	-0.1673
LiH	-2.4572	-2.4485	-2.3460	-0.0087	-0.1112	-0.1025
N2	-9.6722	-9.6705	-9.5358	-0.0017	-0.1365	-0.1347
N2H4	-18.4337	-18.5248	-18.2780	0.0911	-0.1557	-0.2468
NH2	-7.7521	-7.7827	-7.6885	0.0306	-0.0636	-0.0942
NH3	-12.5699	-12.6237	-12.4889	0.0538	-0.0810	-0.1348
NH	-3.5627	-3.5769	-3.5255	0.0142	-0.0372	-0.0514
NO	-6.3758	-6.4087	-6.3095	0.0329	-0.0663	-0.0992
O2	-4.8534	-4.9058	-4.8047	0.0524	-0.0486	-0.1011
OH	-4.4649	-4.4964	-4.4231	0.0315	-0.0418	-0.0733
RMS	/	/	/	0.0507	0.1059	0.1413

Table 4.9: RPA atomization energies in eV for a subset of G2 molecules calculated with VASP. The RPA correlation energies are obtained for 8 Å cells and 800 eV cutoff and added to the HXX energies (20 Å cells and 1000 eV cutoff) found in Table (4.8). The reported results are compared to values of Bates et al. [1] and Ren et al. [40]. The columns $\Delta_{\text{V-B}}$, $\Delta_{\text{V-R}}$ and $\Delta_{\text{B-R}}$ denote the errors Δ(VASP-Bates), Δ(VASP-Ren) and Δ(Bates-Ren) respectively. The corresponding root-mean-square deviation (RMS) is given in the final row.

Molecules	**VASP**	**Furche$_{\mathbf{BSSE}}$**	**Furche**	**Bates**
H2O	-9.6323	-9.6832	-9.7006	-9.7050
Δ(VASP-...)	/	0.0509	0.0683	0.0727

Table 4.10: Comparison of the H_2O RPA atomization energies in eV calculated in VASP and TURBOMOLE (Furche and Bates). The column Furche$_{\mathrm{BSSE}}$ denotes the BSSE corrected energy, while the columns Furche and Bates contain uncorrected results.

With a root-mean-square deviation of 51 meV, the RPA atomization energies are quite not within chemical precision to those of Bates et al. Large discrepancies were found for both BeH and Li_2. This is probably due to too small cells for the BeH and Li_2 molecules as well as for the Be and Li atoms. At the HXX level we found excellent agreement in the atomization energies of both molecules, suggesting that the RPA correlation energy is not converged with respect to the cell size. This is congruent with the results of the cell size test carried out prior. While using the cell size extrapolated correlation energy of BeH decreases the error to 50 meV, we could not extrapolate the Li_2 correlation energy because of its non-linear behaviour. Using the cell size extrapolated correlation energies of LiH and LiF, the atomization energies moreover under-correlate by more than 100 meV compared to Bates et al (see Table (4.6)). Note that Bates et al. obtained their correlation energies extrapolating between the cc-pVQZ and cc-pV5Z (4-5 extrapolation) Gaussian basis sets [1]. Nevertheless, a 5-6 basis set extrapolation is probably required in order to reduce the reported uncertainties at least to a certain extent. Furthermore, Bates et al. did not correct for the basis set superposition error (BSSE) [60] as they claim it to be typically less than 1 kcal/mol for covalent bonds. This error emerges because the basis set used for the molecule is larger than those of the individual atoms. The atoms in the molecule are thus better described than the isolated atoms resulting in a lowering of the molecular energy and a too-large atomization energy. It is assumed that the converged atomization energy is in between the non-corrected and BSSE corrected value.
Besides these molecules involving atoms with extended orbitals, sizable errors are found for H_2O_2 and N_2H_4. Both molecules under-correlate compared to Bates et al. by approximately 100 meV. We can not rule out that these deviations are partly due to BSSE errors in heavy atoms (O, N and F) or the 4-5 extrapolation. We received additional RPA atomization energies for H_2O (private communication with Fillip Furche). Those were calculated in TURBOMOLE using 4-5 basis set extrapolation. In Table (4.10) we see that the non-corrected results of Furche and Bates et al. agree within a few meV. The remaining difference is likely related to different geometries. In addition, we find that our results show better agreement with the BSSE corrected values than without BSSE correction.

Our RPA atomization energies are also compared to results obtained by Ren et al. in 2012, which have been calculated using FHI-aims using tier 4 + a5Z-d basis sets [40]. Those values show much larger discrepancies to both Bates et al. and VASP. In fact our values are usually in between those of Bates et al. and Ren et al., but clearly closer to Bates than Ren. This suggests that the results of Ren are not basis set converged. We conclude that it is technically very challenging to obtain accurate RPA atomization energies.

4.2 RPA atomization energies using RPA-NOs

In the last section, we investigated strategies to obtain accurate RPA atomization energies using a DFT single-particle basis. Since RPA calculations are very expensive using plane-waves, natural orbitals are an obvious choice for the single-particle basis functions. Thus, we investigate the convergence of the RPA atomization energy with respect to the number of natural orbitals used. Further, we evaluated two distinct methods to obtain a set of truncated natural orbitals. The RPA-NOs are the eigenfunctions of the RPA density matrix, which is constructed in a one-shot GW calculation and then diagonalized in the unoccupied subspace. Thus the occupied orbitals are retained and therefore the underlying DFT ground-state is exactly reproduced [42]. The natural orbitals are sorted by their occupation numbers in descending order. Note that we already obtain an RPA correlation energy from the RPA-NO calculation, involving all virtual states. We will use this correlation energy as a basis set limit for the convergence of the natural orbitals. The natural orbitals are then used as basis functions in an RPA calculation. Since they are ordered by their occupation numbers, one simply truncates the list of natural orbitals at a certain point to get a set of basis functions. This procedure is done for various numbers of natural orbitals. The obtained correlation energies are compared to the basis set limit (i.e. the correlation energy evaluated in the complete available virtual space) to see how many natural orbitals are needed to converge the correlation energy within a certain threshold. Note that after truncating the list of natural orbitals, the DFT (or HF) Hamiltonian is diagonalized in the subspace spanned by the truncated natural orbital set. These orbitals span the same space as the truncated set of natural orbitals but allow the use of Brillouin's theorem [42]. Furthermore, the RPA and MP2 code assume that the used orbitals diagonalize the mean field Hamiltonian (be it DFT or HF).
To summarize, RPA natural orbitals are calculated for the molecules and the atoms individually. These sets are truncated and further used to evaluate the RPA correlation energy. The convergence of these correlation energy differences with respect to the number of used natural orbitals is compared to the basis set limit. The main question is how to

truncate the list of natural orbitals. Since we focus on atomization energies (or on the correlation contribution to the atomization energies), one has to construct "equivalent" accurate natural orbital sets for the molecule and the atoms. We decided to evaluate two possible strategies to decide how many natural orbitals are included: (a) use a fixed number of natural orbitals for each occupied state or (b) truncate the list of natural orbitals at a certain minimum occupation number. We refer to these two methods in the following as the fixed basis set and minimum occupation number scheme respectively.
We included a few more molecules from the G2 test set involving 3rd row elements such as ClO, HCl, H_2S, Si_2H_6, SiH_4, H_2S, HCl and PH_3. The natural orbital calculations have been performed with the hard GW potentials evaluated in the last section. We chose a 8 Å cubic cell and a 700 eV plane-wave cutoff. Since the natural orbital evaluation includes a frequency integration one has to be careful to choose an adequate frequency grid. Especially for small band gap systems, many frequency grid points are needed to obtain good natural orbitals. This includes Li, C, O, F, Si, P, S, Cl, NO and OH, where 16 frequency grid points are required for the determination of the NOs. It turns out that for the remaining systems 12 grid points are sufficient.

4.2.1 Fixed basis set scheme

In the first scheme, we chose the number of included natural orbitals to be proportional to the number of occupied states in the majority spin channel. For example, a natural orbital basis set of 32 natural orbitals per occupied state (32NOs/occ) contains 32, 96 and 192 natural orbitals for H, C and C_2H_4 respectively. However, this scheme has some obvious flaws. First of all, the minority spin channel is ignored and the same number of natural orbitals is used to describe these states as for the majority spin channel. Therefore, unnecessarily many natural orbitals are included for the minority spin states. Second, if either the molecule or the individual atoms require more basis functions than the other constituents, a basis set imbalance error is introduced. This is because e.g H is already well described with 32NOs/occ while C_2H_4 requires more basis functions. Since H may already be converged while C_2H_4 is not, an error is introduced lowering the atomization energy. This error can be avoided by increasing the basis set size such that all constituents are equally well converged. However, this defeats the entire purpose of using natural orbitals in the first place. In Fig. (4.4) the convergence of the atomization energy with respect to the number of natural orbitals is shown for C_2H_4 and $Si2_2H_6$.
The correlation contribution to the atomization energy of C_2H_4 in Fig. (4.4a) converges well with increased basis set size and is converged within 30 meV to the basis set limit

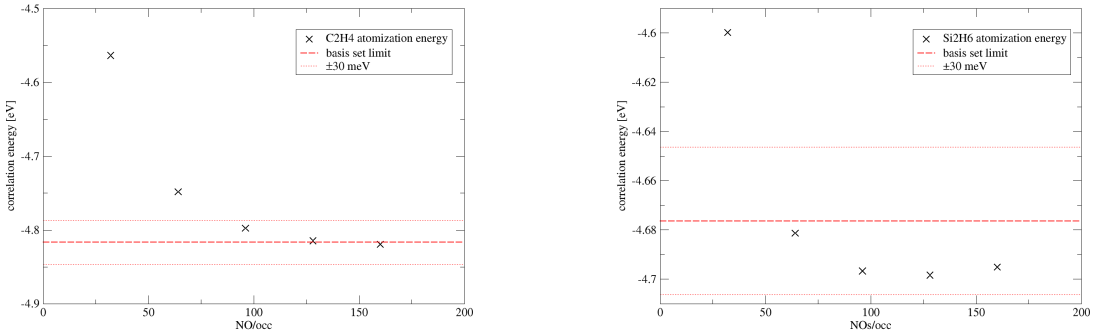

(a) (b)

Figure 4.4: Convergence of the correlation contribution to the atomization energy with respect to the natural orbital basis set size using the fixed basis set scheme evaluated for (a) C_2H_4 and (b) Si_2H_6.

with 92NOs/occ. In Fig. (4.4b) the convergence of the Si2H6 atomization energy is shown. Since hydrogen is probably already converged with 92Nos/occ but the Si2H6 not, a sizable error of ≈20 meV prevails. The calculated correlation energy difference is lower than the basis set limit and will converge from below with an increasing number of natural orbitals. Using this scheme we report converged correlation energy difference within 30 meV to the basis set limit between 64NOs/occ and 92NOs/occ. Because the basis set size is determined by the occupied states in the majority spin channel, in general, unnecessarily many natural orbitals are used to describe the minority spin channel. The extreme example being H with no occupied state in the down spin channel. This results in unnecessary computational effort because those natural orbitals do not need to be included. Further, serious basis set imbalance errors may occur for large molecules or molecules involving many small atoms. Thus we evaluated another method that should avoid these inherent flaws of the fixed basis set scheme.

4.2.2 Minimum occupation number scheme

Since the number of occupied states in the majority spin channel turned out to be no good measure to construct natural orbital basis sets for atomization energies, the occupation numbers appear as the next obvious choice. Recall that the natural orbitals are sorted by their occupation numbers in descending order and these, in many ways, represent their importance in the virtual space. Thus, determining the number of natural orbitals included in the truncated set by setting a minimum required occupation number seems a logical next

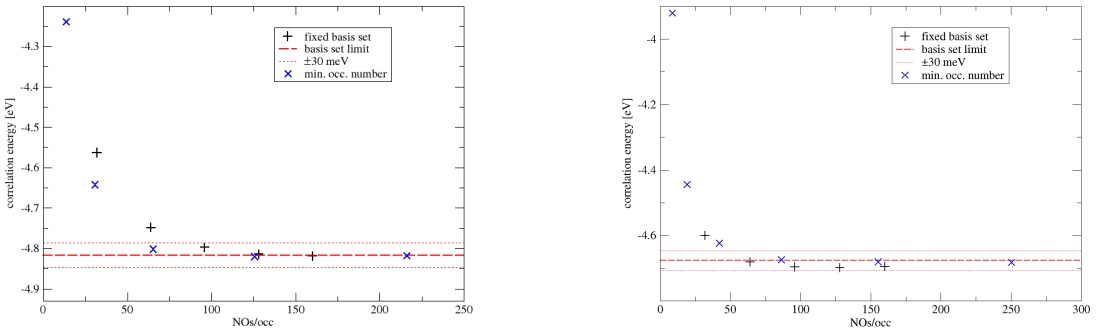

(a) (b)

Figure 4.5: Comparison of the two truncation schemes. The convergence of correlation contribution to the atomization energy with respect to the natural orbital basis set size is evaluated for (a) C_2H_4 and (b) Si_2H_6.

step. This approach naturally treats the up and down spin channel separately, allowing for a different number of natural orbitals for each channel. Therefore, this scheme avoids by design including unnecessarily many natural orbitals for the minority spin channel. This allows for faster calculations as the natural orbital sets are kept as compact as possible. It turns out that also the basis set imbalance error is somewhat avoided or at least mitigated in this approach. Since a minimum occupation number is used to construct the basis sets, this number is in a sense a measure of the accuracy of the truncated natural orbital set. Thus, the truncated sets of the molecule and the atoms should be consistent by design. However, small basis set imbalance errors still may occur but not as severe as for the previous scheme.

To analyze the convergence behavior of the correlation energy differences calculated with natural orbital basis sets that are obtained with the minimum occupation number scheme, we performed calculations with minimum occupation numbers between 10^{-4} to 10^{-9}. To compare this to the previous scheme, we evaluated how many natural orbitals per occupied state of the molecules each basis set corresponds to. The molecule is used as a reference because its basis set will dominate for large molecules and therefore it will be the major cost factor in correlated CI calculations.

In Fig. (4.5) the convergence behavior of the two discussed truncation schemes is compared for C_2H_4 and Si_2H_6. We see that the minimum occupation number scheme converges at least as fast as the previous scheme. This is a property we observed for all molecules. Although a small basis set superposition error of a few meV prevails for Si_2H_6, it is not as severe as in the other scheme. In general, the occupation number method yields converged

correlation energy differences between 60NOs/occ and 92NOs/occ. Keep in mind that although this might sound comparable to the fixed basis set scheme, noticeably fewer natural orbitals are included because the minority spin channel is treated separately and in general fewer natural orbitals are used to describe the individual atoms. Looking at Fig. (4.5b), interpolation of the data sets predicts that the fixed basis set scheme reaches the desired accuracy at ~46NOs/occ, while the occupation number method requires ~58NOs/occ. Nevertheless, the occupation number method is superior as it does not over-correlate as severely as the fixed basis set scheme.
Although this truncation scheme seems promising, there is also a downside. It seems that a well-behaved convergence is not always guaranteed. Especially for small basis sets obtained when using fairly large occupation number thresholds between 10^{-4} and 10^{-5} we sometimes encounter large fluctuations in the correlation energy differences for a few molecules. One example is given in Fig. (4.6).

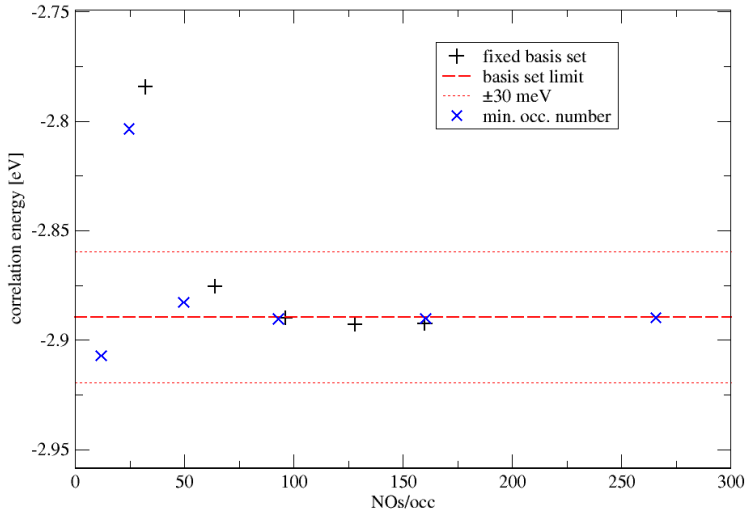

Figure 4.6: Comparison of the two truncation schemes for H_2O. The convergence of the correlation energy contribution to the atomization energy with respect to the natural orbital basis set size is evaluated.

We see that the correlation energy difference of H_2O seems accurate for the 10^{-4} basis set but not for the 10^{-5} set. This is probably due to shell effects, where the number of NOs abruptly increases for the O atoms at 10^{-5}, whereas the NO basis for the molecules remains small. We conclude that the importance measure using occupation numbers does not always work reliably for really small basis sets. Therefore one should always do a proper

convergence analysis to notice and avoid this problem. All in all, this scheme performs better than the fixed basis set scheme. It naturally treats both spin channels independently and thus naturally yields more compact basis sets. Hence it converges as fast as the fixed basis set scheme, and for most of the molecules even slightly faster. Finally, it reduces large basis set imbalance errors as discussed at the beginning of this section, although they are not completely avoided. Fluctuations in the correlation energy differences for small basis sets are no problem as long as one does a carefull convergence analysis. Thus, the minimum occupation number scheme is a reliable method to obtain truncated natural orbital basis sets with a fast convergence for the calculation of atomization energies using post RPA methods.

4.3 Lattice constants of solids using RPA-NOs

Finally, we also calculated lattice constants of a small set of solids using RPA natural orbitals in an RPA calculation. The calculations have been performed for diamond, LiF, BN and Si with a 700 eV energy cutoff using a $4 \times 4 \times 4$ Γ-centered k point mesh. We varied the volume of the unit cell by ±10% around the value obtained using experimental lattice constants. Those are summarized in Tab. (4.11). Note that, since BN forms a layered hexagonal crystal, we decided to vary the distance between its layers not the volume of the unit cell in order to study whether NOs can be used for weak dispersion interactions.

Systems	Crystal	Lattice const.
hBN	hexagonal	6.6612
Diamond	cubic	3.5595
LiF	cubic	4.027
Si	cubic	5.4198

Table 4.11: Experimental lattice constants in Å of BN [61], diamond [62], LiF [63] and Si [64] and the corresponding crystal systems. For BN the lattice constant in the direction c is specified.

For each volume, we performed multiple RPA calculations using between 16NOs/occ and 176NOs/occ. Thus, we obtained multiple sets of RPA total energies using equivalent natural orbital basis set for the different volumes. Using the Murnaghan equation of state [65], the RPA total energies for different crystal volumes can be interpolated to find the ground-state total energy E_0 and the ground-state volume V_0. The equation expresses the energy of a material in terms of its volume and is widely used in solid-state thermodynamics:

$$E(V) = E_0 + B_0 V_0 \left[\frac{1}{B'(B'-1)} \left(\frac{V_0}{V} \right)^{B'-1} + \frac{V}{(B'V_0)} - \frac{1}{B'-1} \right]. \tag{4.3.1}$$

Figure (4.7) shows the convergence of the extrapolated ground-state lattice constants with respect to the number of natural orbitals used in the RPA calculation. They are compared to the lattice constants obtained by a reference HF calculation. We see that for diamond, LiF and Si already 16 natural orbitals per occupied state are enough to converge the lattice constant within 0.3% of the basis set limit. To converge the lattice constant of BN within the given threshold 96 natural orbitals per occupied state are required. Note that for a vdW-system a 1% error is very acceptable. The reason is that the individual layers of BN are held together by van der Waals type forces, i.e. only correlation (HF is purely repulsive). Thus a correlation method is required to properly describe layered systems like BN. Because HF yields no inter-layer binding, there is no reference HF lattice constant in Fig. (4.7a).

While we find an immediate improvement on the lattice constant of diamond and Si by using the RPA, the LiF HF lattice constant is already a good approximation. This is probably due to very weak correlation effects. Thus, at least 80 natural orbitals per occupied state are required to obtain better lattice constants than those provided by HF calculations. In Fig. (4.8) we compare the convergence of the total RPA energy using either natural orbitals or plane-waves as single-particle orbitals in the RPA calculation of BN and diamond. We find that in both cases less natural orbitals are required to obtain converged energies up to a certain threshold. Since correlation effects are less important in diamond compared to BN, less natural orbitals are required to converge the diamond total energy.

We conclude that RPA-NOs are a very useful single-particle basis for RPA calculations on solids. However, since RPA calculations on solids are less expensive than on molecules, their impact is not as significant. Sufficiently accurate lattice constants can be obtained with as few as 16 natural orbitals per occupied state for weakly correlated systems like diamond, LiF or Si and even BN.

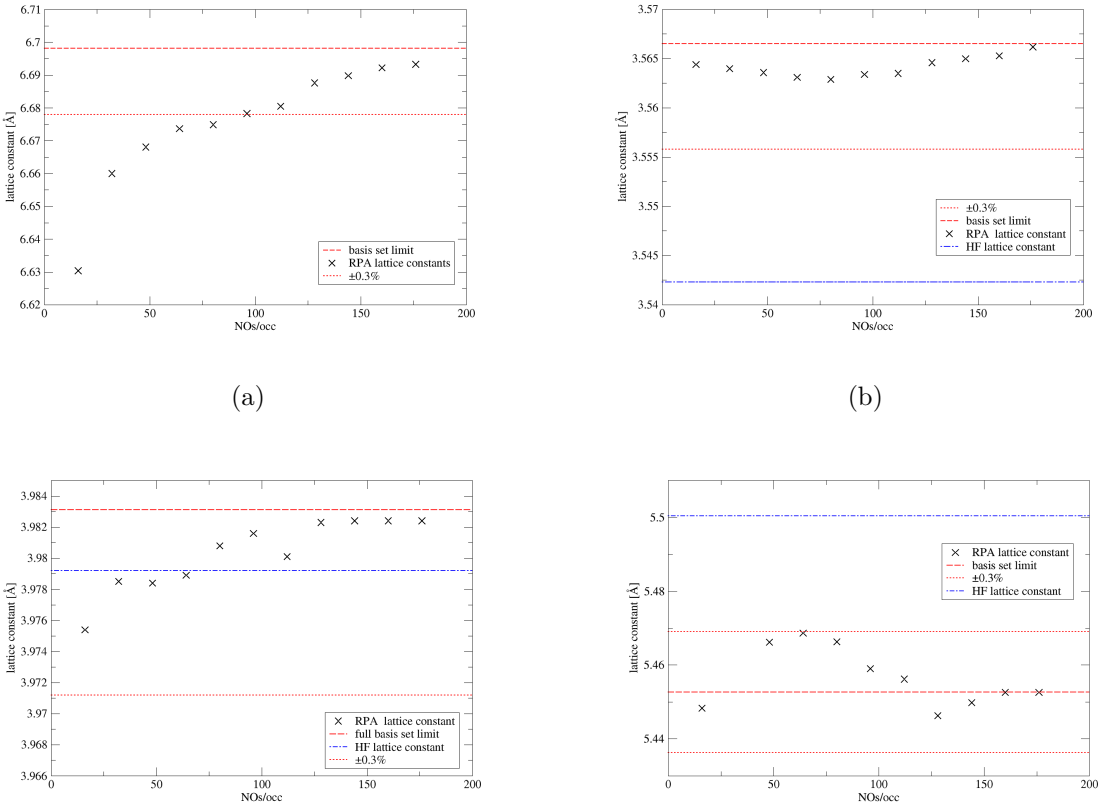

(a) (b)

(c) (d)

Figure 4.7: Convergence of RPA lattice constants (black data-sets) of (a) BN, (b) diamond, (c) LiF and (d) Si with respect to the number of natural orbitals used per occupied state. Furthermore the RPA lattice constants are compared to the HF lattice constants (blue line).

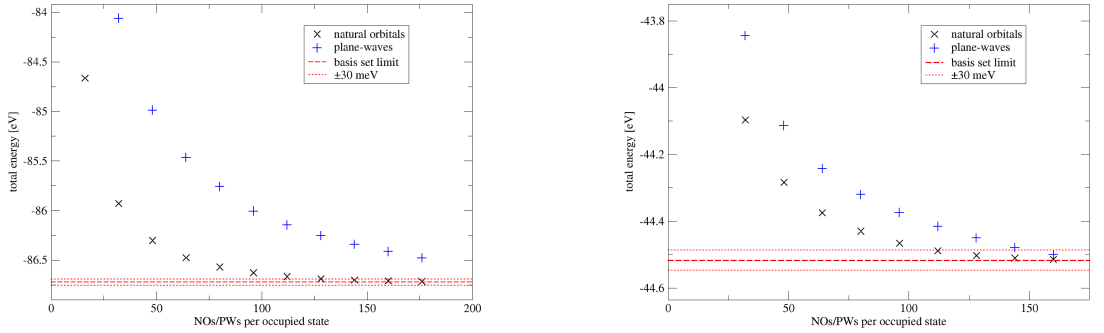

(a) (b)

Figure 4.8: Convergence of RPA total energies towards the basis set limit (red line) using natural orbitals (black data-sets) and plane-waves (blue data-sets) for (a) BN and (b) diamond.

Conclusion

The random-phase approximation allows for a low complexity treatment of the correlation energy in molecules and solids. Now that it is computationally feasible it has found widespread use and hence bench-marks between different implementations are important. Our reported PBE and HXX@PBE atomization energies show great agreement with the results published by Paier et al. and Bates et al. using Gaussian basis set codes. Despite our RPA results not agreeing to within chemical precision (1 kcal/mol) with the values of to Bates et al., they are still in quite good agreement if one considers the lack of basis set superposition error (BSSE) corrections. Furthermore, our present values clearly demonstrate that the reported FHI-aims values for RPA energies by Ren et al. are inadequate with error-bars beyond 5 kcal/mol. It has been shown that accounting for the BSSE correction in atomization energies yields results in somewhat closer agreement with the ones calculated in VASP. In addition, we have observed that the cell size has great impact on the correlation energy of atoms with extended orbitals like Be and Li. Improved atomization energies for molecules involving these atoms can be obtained by using larger cells and extrapolating the correlation energies to the infinite cell size limit. Accounting for the cell size dependence of the correlation energy and comparing it to cc-pV5Z - cc-pV6Z basis set extrapolated and BSSE corrected atomization energies, we are confident that in future assessments chemical precision between the VASP and TURBOMOLE RPA implementations can be achieved. In summary, the presented tests have shown that the set of hard GW potentials is a suitable choice for RPA calculations, yielding acceptably accurate atomization energies.

Since correlated methods beyond RPA are typically rather expensive, RPA natural orbitals are promising single-particle basis functions. We observed that, in general, less than 100 natural orbitals per occupied state are required to obtain converged RPA correlation energies. This suggests that the computational effort of more sophisticated correlated methods can be significantly decreased by employing natural orbitals. The number of required natural orbitals can be even further reduced by using the minimum occupation number truncation scheme. This has proven useful since it not only provides a compact natural orbital basis set but also because it mitigates the basis set imbalance error that causes small natural orbital basis sets to yield over-correlated atomization energies. Further investigations, including more molecules and other correlated methods (e.g. MP2 as well as auxiliary field quantum Monte Carlo) need to be carried out to verify that it is indeed a viable truncation scheme. Finally, we found that for the considered bulk systems as few as

16 natural orbitals are required to accurately describe their lattice constants. Thus, natural orbitals are potentially exceedingly useful for highly accurate calculations on molecules and solids.

References

[1] J. E. Bates and F. Furche, "Communication: Random phase approximation renormalized many-body perturbation theory," *The Journal of chemical physics*, vol. 139, no. 17, pp. 171103–171103, 2013.

[2] A. Savin, F. Colonna, and R. Pollet, "Adiabatic connection approach to density functional theory of electronic systems," *International journal of quantum chemistry*, vol. 93, no. 3, pp. 166–190, 2003.

[3] A. Szabo, *Modern quantum chemistry : introduction to advanced electronic structure theory*. Mineola, NY: Dover Publ., 1. ed., rev.. ed., 1996.

[4] J. P. Perdew and S. Kurth, *Density Functionals for Non-relativistic Coulomb Systems in the New Century*, pp. 1–55. Springer Berlin Heidelberg, 2003.

[5] P. Hohenberg and W. Kohn, "Inhomogeneous electron gas," *Phys. Rev.*, vol. 136, pp. B864–B871, Nov 1964.

[6] W. Kohn and L. J. Sham, "Self-consistent equations including exchange and correlation effects," *Phys. Rev.*, vol. 140, pp. A1133–A1138, Nov 1965.

[7] W. Kohn, *Fundamentals of density functional theory*, pp. 1–7. Springer Berlin Heidelberg, 1998.

[8] R. G. Parr and W. Yang, "Density-functional theory of the electronic structure of molecules," *Annual Review of Physical Chemistry*, vol. 46, no. 1, pp. 701–728, 1995.

[9] O. Gunnarsson and B. I. Lundqvist, "Exchange and correlation in atoms, molecules, and solids by the spin-density-functional formalism," *Phys. Rev. B*, vol. 13, pp. 4274–4298, May 1976.

[10] W. Kohn, A. D. Becke, and R. G. Parr, "Density functional theory of electronic structure," *The Journal of Physical Chemistry*, vol. 100, no. 31, p. 12974–12980, 1996.

[11] R. M. Dreizler, *Density functional theory : an approach to the quantum many-body problem*. Berlin [u.a.]: Springer, 1990.

[12] R. M. Martin, *Density functional theory: foundations*, p. 119–134. Cambridge University Press, 2004.

[13] J. P. Perdew, K. Burke, and M. Ernzerhof, "Generalized gradient approximation made simple," *Phys. Rev. Lett.*, vol. 77, pp. 3865–3868, Oct 1996.

[14] M. Ernzerhof and G. E. Scuseria, "Assessment of the perdew–burke–ernzerhof exchange-correlation functional," *The Journal of chemical physics*, vol. 110, no. 11, pp. 5029–5036, 1999.

[15] A. D. BECKE, "Density-functional thermochemistry. iii: The role of exact exchange," *The Journal of chemical physics*, vol. 98, no. 7, pp. 5648–5652, 1993.

[16] A. D. BECKE, "A new mixing of hartree-fock and local density-functional theories," *The Journal of chemical physics*, vol. 98, no. 2, pp. 1372–1377, 1993.

[17] A. D. Becke, "Density-functional exchange-energy approximation with correct asymptotic behavior," *Phys. Rev. A*, vol. 38, pp. 3098–3100, 1988.

[18] C. Lee, W. Yang, and R. G. Parr, "Development of the colle-salvetti correlation-energy formula into a functional of the electron density," *Phys. Rev. B*, vol. 37, pp. 785–789, 1988.

[19] S. H. Vosko, L. Wilk, and M. Nusair, "Accurate spin-dependent electron liquid correlation energies for local spin density calculations: a critical analysis," *Canadian Journal of Physics*, 1980.

[20] S. Kurth and J. P. Perdew, "Role of the exchange-correlation energy: Nature's glue," *International journal of quantum chemistry*, vol. 77, no. 5, pp. 814–818, 2000.

[21] J. Harris and R. O. Jones, "The surface energy of a bounded electron gas," *Journal of physics. F, Metal physics*, vol. 4, no. 8, pp. 1170–1186, 1974.

[22] W. Yang, "Generalized adiabatic connection in density functional theory," *The Journal of chemical physics*, vol. 109, no. 23, pp. 10107–10110, 1998.

[23] P. Politzer and J. S. Murray, "The hellmann-feynman theorem: a perspective," *Journal of molecular modeling*, vol. 24, no. 9, pp. 1–7, 2018.

[24] E. Schrödinger, "Quantisierung als eigenwertproblem," *Annalen der Physik*, vol. 385, no. 13, pp. 437–490, 1926.

[25] H. Hellmann, "Zur rolle der kinetischen elektronenenergie für die zwischenatomaren kräfte," *Zeitschrift für Physik*, vol. 85, no. 3, pp. 180–190, 1933.

[26] H. Hellmann, *Einführung in die Quantenchemie : mit 35 Tabellen*. Deuticke, 1937.

[27] R. P. Feynman, "Forces in molecules," *Phys. Rev.*, vol. 56, pp. 340–343, 1939.

[28] J. Esteve, F. Falceto, and C. García Canal, "Generalization of the hellmann–feynman theorem," *Physics Letters A*, vol. 374, no. 6, pp. 819–822, 2010.

[29] K. Burke, *Digging into the Exchange-Correlation Energy: The Exchange-Correlation Hole*, pp. 19–29. Springer US, 1998.

[30] F. Furche, "Developing the random phase approximation into a practical post-kohn-sham correlation model," *The Journal of chemical physics*, vol. 129, no. 11, pp. 114105–114105–8, 2008.

[31] X. Ren, P. Rinke, C. Joas, and M. Scheffler, "Random-phase approximation and its applications in computational chemistry and materials science," *Journal of materials science*, vol. 47, no. 21, pp. 7447–7471, 2012.

[32] H. Eshuis, J. E. Bates, and F. Furche, "Electron correlation methods based on the random phase approximation," *Theoretical chemistry accounts*, vol. 131, no. 1, pp. 1–18, 2012.

[33] H. B. Callen and T. A. Welton, "Irreversibility and generalized noise," *Phys. Rev.*, vol. 83, pp. 34–40, 1951.

[34] Y. B. Band and Y. Avishai, *Quantum Mechanics with Applications to Nanotechnology and Information Science*. Elsevier Science & Technology, 2012.

[35] F. Furche and T. Van Voorhis, "Fluctuation-dissipation theorem density-functional theory," *The Journal of chemical physics*, vol. 122, no. 16, pp. 164106–164106, 2005.

[36] G. C. Wick, "Properties of bethe-salpeter wave functions," *Phys. Rev.*, vol. 96, pp. 1124–1134, 1954.

[37] E. Runge and E. K. U. Gross, "Density-functional theory for time-dependent systems," *Phys. Rev. Lett.*, vol. 52, pp. 997–1000, 1984.

[38] F. Furche, "Molecular tests of the random phase approximation to the exchange-correlation energy functional," *Phys. Rev. B*, vol. 64, p. 195120, Oct 2001.

[39] M. Petersilka, U. J. Gossmann, and E. K. U. Gross, "Excitation energies from time-dependent density-functional theory," *Phys. Rev. Lett.*, vol. 76, pp. 1212–1215, 1996.

[40] X. Ren, P. Rinke, V. Blum, J. Wieferink, A. Tkatchenko, A. Sanfilippo, K. Reuter, and M. Scheffler, "Resolution-of-identity approach to hartree-fock, hybrid density functionals, rpa, mp2 and gw with numeric atom-centered orbital basis functions," *New journal of physics*, vol. 14, no. 5, 2012.

[41] R. D. Mattuck and H. Chang, "A guide to feynman diagrams in the many-body problem," *Physics today*, vol. 22, no. 5, pp. 87–89, 1969.

[42] B. Ramberger, Z. Sukurma, T. Schäfer, and G. Kresse, "Rpa natural orbitals and their application to post-hartree-fock electronic structure methods," *The Journal of chemical physics*, vol. 151, no. 21, pp. 214106–214106, 2019.

[43] A. D. McLACHLAN and M. A. BALL, "Time-dependent hartree—fock theory for molecules," *Rev. Mod. Phys.*, vol. 36, pp. 844–855, Jul 1964.

[44] G. E. Scuseria, T. M. Henderson, and I. W. Bulik, "Particle-particle and quasiparticle random phase approximations: connections to coupled cluster theory," *The Journal of chemical physics*, vol. 139, no. 10, pp. 104113–104113, 2013.

[45] M. Kaltak, J. c. v. Klimeš, and G. Kresse, "Cubic scaling algorithm for the random phase approximation: Self-interstitials and vacancies in si," *Phys. Rev. B*, vol. 90, p. 054115, Aug 2014.

[46] J. Harl, L. Schimka, and G. Kresse, "Assessing the quality of the random phase approximation for lattice constants and atomization energies of solids," *Phys. Rev. B*, vol. 81, p. 115126, Mar 2010.

[47] S. Kurth and J. P. Perdew, "Density-functional correction of random-phase-approximation correlation with results for jellium surface energies," *Phys. Rev. B*, vol. 59, pp. 10461–10468, Apr 1999.

[48] M. Fuchs, Y.-M. Niquet, X. Gonze, and K. Burke, "Describing static correlation in bond dissociation by kohn-sham density functional theory," *The Journal of chemical physics*, vol. 122, no. 9, pp. 094116–094116, 2005.

[49] A. Heßelmann and A. Görling, "Correct description of the bond dissociation limit without breaking spin symmetry by a random-phase-approximation correlation functional," *Phys. Rev. Lett.*, vol. 106, p. 093001, Feb 2011.

[50] P.-O. Löwdin, "Quantum theory of many-particle systems. i. physical interpretations by means of density matrices, natural spin-orbitals, and convergence problems in the method of configurational interaction," *Phys. Rev.*, vol. 97, pp. 1474–1489, Mar 1955.

[51] E. R. Davison, "Properties and uses of natural orbitals," *Reviews of modern physics*, vol. 44, no. 3, pp. 451–464, 1972.

[52] C. F. Bender and E. R. Davidson, "A natural orbital based energy calculation for helium hydride and lithium hydride," *The Journal of Physical Chemistry*, vol. 70, no. 8, pp. 2675–2685, 1966.

[53] K. H. Thunemann, J. Römelt, S. D. Peyerimhoff, and R. J. Buenker, "A study of the convergence in iterative natural orbital procedures," *International Journal of Quantum Chemistry*, vol. 11, no. 5, pp. 743–752, 1977.

[54] D. Feller and K. A. Peterson, "Re-examination of atomization energies for the gaussian-2 set of molecules," *The Journal of chemical physics*, vol. 110, no. 17, pp. 8384–8396, 1999.

[55] N. Nemec, M. D. Towler, and R. J. Needs, "Benchmark all-electron ab initio quantum monte carlo calculations for small molecules," *The Journal of chemical physics*, vol. 132, no. 3, pp. 034111–034111, 2010.

[56] G. Kresse and D. Joubert, "From ultrasoft pseudopotentials to the projector augmented-wave method," *Phys. Rev. B*, vol. 59, pp. 1758–1775, Jan 1999.

[57] T. H. Dunning, "Gaussian basis sets for use in correlated molecular calculations. i. the atoms boron through neon and hydrogen," *The Journal of chemical physics*, vol. 90, no. 2, pp. 1007–1023, 1989.

[58] J. Harl and G. Kresse, "Cohesive energy curves for noble gas solids calculated by adiabatic connection fluctuation-dissipation theory," *Phys. Rev. B*, vol. 77, p. 045136, Jan 2008.

[59] J. Paier, R. Hirschl, M. Marsman, and G. Kresse, "The perdew-burke-ernzerhof exchange-correlation functional applied to the g2-1 test set using a plane-wave basis set," *The Journal of chemical physics*, vol. 122, no. 23, pp. 234102–234102, 2005.

[60] M. Gutowski, J. Van Lenthe, J. Verbeek, F. Van Duijneveldt, and G. Chałasinski, "The basis set superposition error in correlated electronic structure calculations," *Chemical physics letters*, vol. 124, no. 4, pp. 370–375, 1986.

[61] "Boron nitride (bn) lattice parameters: Datasheet from landolt-börnstein - group iii condensed matter · volume 41a1α: "group iv elements, iv-iv and iii-v compounds. part a - lattice properties" in springermaterials (https://doi.org/10.1007/10551045_6)." accessed 2021-08-17.

[62] "Diamond (c dia) crystal structure: Datasheet from "pauling file multinaries edition – 2012" in springermaterials (https://materials.springer.com/isp/crystallographic/docs/sd_1939112)." accessed 2021-08-17.

[63] "Lif crystal structure: Datasheet from "pauling file multinaries edition – 2012" in springermaterials (https://materials.springer.com/isp/crystallographic/docs/sd_1021390)." accessed 2021-08-17.

[64] "Silicon (si) lattice parameters: Datasheet from landolt-börnstein - group iii condensed matter · volume 41a1α: "group iv elements, iv-iv and iii-v compounds. part a - lattice properties" in springermaterials (https://doi.org/10.1007/10551045_198)." accessed 2021-08-17.

[65] B. Silvi and P. d'arco, *Modelling of Minerals and Silicated Materials*. Springer Netherlands, 2002.